Infiltration of CD4+ lymphocytes into the brain contributes to neurodegeneration in a mouse model of Parkinson disease.

Vanessa Brochard, Béhazine Combadière, Annick Prigent, Yasmina Laouar, Aline Perrin, Virginie Beray-Berthat, Olivia Bonduelle, Daniel Alvarez-Fischer, Jacques Callebert, Jean-Marie Launay, et al.

Brain infiltration of CD4 lymphocytes contributes to neurodegeneration in Parkinson's disease model

Vanessa Brochard[1,2], Béhazine Combadière[3], Annick Prigent[1,2], Yasmina Laouar[4], Aline Perrin[1,2], Virginie Beray-Berthat[1,2], Olivia Bonduelle[3], Daniel Alvarez-Fischer[1,2], Jacques Callebert[6], Jean-Marie Launay[6], Charles Duyckaerts[1,2], Richard A. Flavell[4,5], Etienne C. Hirsch[1,2] & Stéphane Hunot[1,2]

[1]INSERM, UMR_S679, Experimental Neurology and Therapeutics, Hôpital de la Salpêtrière, F-75013, Paris, France.
[2]UPMC, Univ Paris 06, UMR_S679, F-75005, Paris, France.
[3]INSERM U543, Université Pierre et Marie Curie, Univ Paris 06, F-75005, Paris, France.
[4]Department of Immunobiology and [5]Howard Hughes Medical Institute, Yale University School of Medicine, New Haven, CT 06520, USA.
[6]CR Claude Bernard, IFR6, Service de Biochimie, Hôpital Lariboisière, AP-HP, Paris 75010, France.

The authors have declared that no conflict of interest exists.

Address correspondence to Stéphane Hunot or Etienne C. Hirsch, INSERM UMR 679, Hôpital de la Salpêtrière, 47 Bd de l'Hôpital, 75013 Paris, France. Phone: 33-142162172 or 33-142162202. Fax: 33-144243658. E-mail: stephane.hunot@upmc.fr or etienne.hirsch@upmc.fr

Nonstandard abbreviations used:

α-Syn: α-synuclein

BBB: blood brain barrier

DN: dopamine-containing neurons

GFAP: glial fibrillary acidic protein

Gld: Fas ligand-mutated generalized lymphoproliferative

MPTP: 1-methyl-4-phenyl-1,2,3,6-tetrahydropyridine

PCNA: proliferating cell nuclear antigen

PD: Parkinson's disease

SNpc: substantia nigra pars compacta

T_C: cytotoxic T-cell

T_H: helper T-cell

TH: tyrosine hydroxylase

ABSTRACT

Parkinson's disease (PD) is a neurodegenerative disorder characterized by a loss of dopamine-containing neurons. While there is mounting evidence to suggest that innate immunity, primarily associated with activated microglial cells, significantly contributes to dopaminergic cell death, the pathogenic role of the adaptive immune system in PD remains enigmatic. Here, we show that $CD8^+$ and $CD4^+$ T-cells, but not B-cells, invade the brain in *postmortem* PD specimens and in the 1-methyl-4-phenyl-1,2,3,6-tetrahydropyridine (MPTP) mouse model of PD during the course of neuronal degeneration. We further demonstrate that removal of mature T lymphocytes in two different immunodeficient mouse models (*Rag1*$^{-/-}$ and *Tcrb*$^{-/-}$) markedly attenuates MPTP-induced dopaminergic cell death. Importantly, T-cell-mediated dopaminergic toxicity is almost exclusively arbitrated by $CD4^+$ T-cells and requires the expression of Fas ligand but not IFN-γ. Altogether, our data provide a rationale for targeting the adaptive arm of the immune system as a therapeutic strategy in PD.

INTRODUCTION

Parkinson's disease is a neurodegenerative disorder characterized by the loss of dopamine-containing neurons (DNs) in the substantia nigra pars compacta (SNpc). Except for rare genetic forms, PD is a sporadic condition of unknown cause. Yet, several scenarios regarding the mechanisms by which DNs degenerate have been suggested including mitochondrial dysfunction, oxidative stress and the impairment of protein degradation machinery (1). In addition to these well established pathomechanisms, there is mounting evidence from epidemiological, *postmortem* and animal studies to suggest that innate neuroinflammatory processes associated with glial cell activation participate in the progression of DN cell death (2-6).

Far more enigmatic is the putative role of the adaptive immune system in PD pathogenesis. While several changes in cellular and humoral immune responses have been described in the peripheral immune system of PD patients, it remains unclear whether these alterations are primarily involved in the etiogenesis of PD or simply reflect secondary consequences of nigrostriatal pathway injury (5). Up to now, the hypothesis that the cellular arm of the adaptive immune system plays a role in neurodegeneration has been hampered by the fact that no clear demonstration of a prominent involvement of leukocytes at the site of neuronal injury has been provided in PD. Yet, the reports many years ago that 1) cytotoxic T-cells (T_C) can be massively found in PD SN (7) and 2) the density of IFN-γ-positive cells is markedly increased in PD brains (8) suggest that T-cell brain recruitment may be associated with nigrostriatal pathway injury in PD. In support of this view is the demonstration that the accumulation of T-cells in the brain can be stimulated in mouse by 1-methyl-4-phenyl-1,2,3,6-tetrahydropyridine (MPTP)-induced DN injury (9). Yet, whether

this immune response truly contributes to neurodegeneration, and, if so, by what mechanisms, remains to be established.

In this study we sought to determine whether PD is associated with leukocyte brain infiltration within the affected SN region and, if so, whether this process contributes to DN degeneration. We found that both $CD8^+$ and $CD4^+$ T-cells significantly invade the SN in *postmortem* PD specimens and in MPTP-intoxicated mice. We also show that removal of $CD4^+$ but not of $CD8^+$ T-cells in mouse greatly reduced MPTP-induced nigrostriatal DN cell death. Finally, we further demonstrate that the deleterious activity of infiltrated $CD4^+$ T-cells involved the Fas/FasL pathway but not IFN-γ production.

RESULTS

Lymphocyte brain infiltration in PD patients

To test the possibility that leukocytes infiltrate the brain parenchyma of PD patients, we performed immunohistochemical staining for various leukocyte-specific markers (10) on *postmortem* human brain (for antibody description, see Supplemental Table 1). Positive staining was observed for CD8 and CD4 but not for B-cell and natural killer cell markers. Within the SNpc, $CD8^+$ and $CD4^+$ T-cells were found either in close contact with blood vessels or in the vicinity of melanized DNs (Figure 1, A and B). These cells displayed a typical lymphocyte morphology that was further confirmed by electron microscopy analysis. At the ultrastructural level, parenchymal CD8+ T-cells displayed small cytoplasmic volume, membrane-type CD8 staining and, in some cases, uropod-like cytoplasmic extension usually involved in T-cell motility (Figure 1C). Importantly, quantitative analysis revealed a significant increase (10 fold in average) in the density of $CD8^+$ and $CD4^+$ T-cells in the SNpc, but not in the non-lesioned red nucleus, from PD patients compared to age-matched control subjects (Figure 1D, and Supplemental Table 2).

MPTP-induced DN lesion stimulates extravasation of lymphocytes into the brain

The above data suggest that migration of peripheral lymphocytes within the central nervous system is associated with nigrostrital pathway injury in PD. Yet, although *postmortem* studies in humans are essential to establish that immune cell infiltration is characteristic of the disease, they cannot provide information about the dynamic and functional relevance of such mechanisms. To address this issue, we conducted *in vivo* experiments using the well-characterized MPTP-intoxicated mouse model of PD (1). Although shortcoming, this non-

invasive model provides a unique mean to study non-cell autonomous pathomechanisms as it recapitulates many of the hallmarks of PD including DN loss, attenuation of striatal dopamine and glial cell-associated inflammatory processes. To easily track the migration of peripheral leukocyte independently of their phenotypic traits, we first used a passive transfer strategy which consisted in transferring GFP-tagged T- or B-cells into recombinase activating gene 1 (*Rag1*)-deficient mice which lack mature lymphocytes. Recipient animals with reconstituted lymphoid organs were then treated with MPTP or saline solution (Figure 2A, and Supplemental Figure 2). Unlike GFP^+ B-cells (data not shown), we found GFP^+ T-cells in the SNpc and striatum after MPTP treatment (Figure 2, B and C). Most, if not all, other brain structures but DN-containing regions were devoid of T-cell infiltrate, indicating the region specific extravasation of these immune cells (Supplemental Figure 3). Brain sections immunostained for tyrosine hydroxylase (TH) show GFP^+ T-cells within the SNpc clustered in close proximity to TH-expressing DNs (Figure 2D). Furthermore, infiltrated T-cells had clearly transmigrated through the brain parenchyma since most of them were found to be excluded from the lumen of blood vessels identified by Glut-1 immunostaining (Figure 2D). Finally, both $CD8^+$ and $CD4^+$ T-cell subtypes were found to be recruited (Figure 2D).

To ensure that the brain infiltration of T-cells observed in our graft-based experimental model was not merely an artefact related to the methodology, we looked at leukocyte transmigration in MPTP-intoxicated C57Bl/6J inbred mice using immunohistochemistry for the T-cell specific marker CD3. In these conditions, a similar T-cell infiltration process was observed (Figure 2E). When compared to the time course of glial cell activation, $CD3^+$ T-cell brain infiltration was found to arise after the increase of $CD11b^+$ microglial cells (i.e. 12 hours post-MPTP intoxication) but concomitantly with astrogliosis (Supplemental Figure 4).

Consistent with our *postmortem* findings, nigral CD8+ T-cells were more abundant than $CD4^+$ T-cells and transmigration occurred at day 2 post-treatment, increased continuously for up to 7 days and had totally ceased at 21 days (Figure 2E). Such dynamics are therefore compatible with a possible role of activated microglial cells in the brain region-specific recruitment of T cells.

The continuous nigral accumulation of T-cells indicates that lymphocytes could clonally expand into the brain parenchyma. To test such a possibility, we surveyed the expression of proliferating cell nuclear antigen (PCNA), taken as a marker of dividing cells, at 0.5, 1, 2, 4 and 7 days after the last MPTP injection. As shown in Figure 2F, while we observed numerous PCNA-positive cells in the SNpc after MPTP intoxication, none of them were found to co-localize with either GFP^+ T-cells or glial fibrillary acidic protein (GFAP)-positive astrocytes at all the time points analyzed. Instead, most of these cells also expressed the myeloid marker CD11b, suggesting that infiltrated macrophages and/or resident microglial cells multiply at the site of injury. Thus, accumulation of T-cells may indicate a continuous extravasation process at least up to 7 days after neurotoxin exposure. Yet, the number of CD3+ T cells within the SNpc was found to dramatically decrease shortly after this accumulation i.e. at day 9 (Supplemental Figure 5A) raising the possibility that they could be rapidly eliminated by apoptotic cell death due to regulatory mechanisms aimed at terminating the immune response. To test this, we looked for morphological criteria as well as molecular changes indicative of apoptosis in the entire SNpc and VTA of animals sacrificed 7 and 9 days after systemic MPTP administration. Immunohistochemistry for CD3 coupled with thionin counterstaining revealed the presence of apoptotic cells characterized by shrinkage of cellular body, chromatin condensation, and presence of distinct, round, well-defined chromatin clumps (Supplemental Figure 5B).

Whereas apoptotic cells were found in all MPTP-treated mice analyzed at day 7 and 9 (n=10 and 5, respectively), they were not observed in saline-injected controls. In few instances, these cells have retained some CD3 staining attesting their T cell origin (Supplemental Figure 5C). Additional evidences for T cell apoptosis were obtained from double immunofluorescent staining for CD3 and activated caspase-3. Thus, some CD3+ T cells were found to be positive for the p17 fragment of activated caspase-3 (Supplemental Figure 5D).

Since previous report indicated that the blood–brain barrier (BBB) may be dysfunctional in PD patients (11), we examined whether MPTP-associated BBB disruption could account for a passive entry of lymphocytes into the brain. A time course of BBB leakage from 6 hours to 7 days after MPTP administration was determined by assessing serum albumin and immunoglobulin extravasation. Our data reveal that MPTP induces a widespread and transitory serum protein leakage (detectable at 6 hours but absent from 12 hours after MPTP) contrasting therefore with the cell type- and region-specific leukocyte extravasation process (Figure 3A). To further explore the mechanism of T-cell extravasation we surveyed the expression of intercellular adhesion molecule-1 (ICAM-1/CD54), an immunoglobulin-like cell adhesion molecule involved in leukocyte adherence and transendothelial migration at sites of inflammation (12). Whereas CD54 was barely detectable in controls (data not shown), we observed a marked increase in CD54 immunostaining within the SNpc at the site of T-cell infiltration following MPTP intoxication (Figure 3B). Blood vessels, glial cells and T-cells were all intensely positive, indicating possible cross-interactions between these cellular actors.

Mice deficient in cell-mediated immunity are more resistant to MPTP

Investigations dedicated to unravel the role of infiltrated T-cells in various models of neuronal injury have led to opposite conclusions (13, 14). To determine whether T-cell accumulation in the SNpc following MPTP intoxication is beneficial or harmful to DNs, we compared the effects of the toxin in T-cell antigen receptor beta gene mutant mice lacking mature T lymphocytes (*Tcrb*$^{-/-}$) (15) and in their wild-type (WT) littermates. We found that whereas only 72% of the nigral TH+ DNs survived MPTP injection in WT mice, 91% of these neurons survived in *Tcrb*$^{-/-}$ mice treated with a similar MPTP regimen (Figure 4, A and B). Importantly, the decrease in MPTP-induced DN loss in *Tcrb*$^{-/-}$ mice correlated with a reduction in the number of infiltrated T-cells to a level similar to that of saline-injected animals (Figure 4C). Residual T-cell infiltration in *Tcrb*$^{-/-}$ mice may come from the small number (about 8% of the WT level) of cells remaining in the thymus of these mutants (15).

Given the apparent harmful behavior of infiltrated T-cells, we next investigated whether CD8^{+} and/or CD4^{+} T-cells could mediate such a detrimental function. To that end, we intoxicated mice homozygous for either a *Cd8a* or a *Cd4* targeted mutation characterized by a deficiency in functional cytotoxic and helper T-cells (T_H), respectively (16, 17). Whereas MPTP induced a comparable level of DN cell death in *Cd8a*$^{-/-}$ mice as in WT littermates, we observed a marked reduction in TH^{+} cell loss in *Cd4*$^{-/-}$ mice (Figure 4, A and B). Interestingly, the rate of DN survival in *Cd4*$^{-/-}$ mice was comparable to that of *Tcrb*$^{-/-}$ animals, suggesting that most of the deleterious outcome associated with infiltrated T-cells is mediated by the CD4^{+} T_H cell subset. In support of this idea, susceptible WT and *Cd8a*$^{-/-}$ mice exhibited a similar number of infiltrated CD4^{+} T-cells following MPTP exposure (Figure 4C). However, there were no significant differences in the extent of loss in striatal levels of dopamine, DOPAC (3-4-dihydroxyphenylacetic acid) and HVA (homovanillic acid) between mutant mice and their wild-type littermates after the administration of MPTP

implying that striatal T-cell infiltration is not a major component of dopaminergic fibber injury (Table 1). Importantly, reduced MPTP metabolism in mutant mice is not likely to account for the observed neuroprotection as striatal MPP+ content after a single systemic MPTP injection did not differ between genotypes (Table 2). Moreover, consistent with the partial resistance of *Tcrb*$^{-/-}$ and *Cd4*$^{-/-}$ mice to MPTP, mid-term (2-7 days) microglial cell activation was almost completely abolished in mutant mice (Figure 4B).

The Fas/FasL pathway is required for CD4 T cell-dependent DN toxicity

The finding that CD4-deficient mice are partially protected against MPTP-induced injury suggests that T_H cell-mediated deleterious mechanisms are engaged and instrumental in DN demise. Cytokines, including IFN-γ, and membrane bound ligands, such as FasL, represent two major classes of molecules mediating effector functions of CD4 T_H cells (e.g. macrophage activation). Interestingly, it has been shown that IFN-γ was a contributing factor in the death of DNs by regulating microglial activity (18). In fact, we found that IFN-γ expression was up-regulated in the ventral midbrain 2 days after MPTP exposure, which coincided with the first wave of $CD4^+$ T-cell brain infiltration (Supplemental Figure 6A). To analyze the putative deleterious role of lymphocyte-derived IFN-γ, we passively transferred total splenocytes isolated from either WT or IFN-γ-deficient mice into recipient *Rag1*$^{-/-}$ animals. Consistent with the deleterious role of T-cells as previously evidenced in *Tcrb*$^{-/-}$ mice, we noticed that MPTP-induced injury in immunodeficient *Rag1*$^{-/-}$ mice was significantly less severe than in WT littermates (Figure 5, A and B). Importantly, this partial resistance was completely reversed when spleen cells from either WT or *Ifn-γ*$^{-/-}$ mice were passively transferred prior to MPTP intoxication (Figure 5A). Thus, lymphocyte-derived INF-γ is not likely to be required for T cell-mediated DN cell death. In support to this

assertion, *Ifn-γ*$^{-/-}$ mice and their WT littermates were found to be equally sensitive to MPTP-induced DA cell death using identical intoxication paradigm (Supplemental Figure 6B). Therefore, we next considered the involvement of a Fas-based mechanism. To test this, we took advantage of the Fas ligand-mutated generalized lymphoproliferative (*gld*) mice that bear a point mutation in the extracellular domain of Fas ligand (FasL/CD95L) resulting in a dramatic decrease of affinity to its receptor Fas (19). Thus, we compared the MPTP susceptibility of *Rag1*$^{-/-}$ recipients that received spleen cells from either *gld* or C57Bl/6J donors (designated *gld* rec. *Rag1*$^{-/-}$ and WT rec. *Rag1*$^{-/-}$, respectively). In WT rec. *Rag1*$^{-/-}$ mice, MPTP caused as much DN loss as in WT animals (Figure 5, A, B and C). In sharp contrast, both non-reconstituted *Rag1*$^{-/-}$ and *gld* rec. *Rag1*$^{-/-}$ mice exposed to a similar dose of MPTP exhibited a significantly smaller reduction in the number of nigral DNs (Figure 5, B and C). The protection gained in *gld* rec. *Rag1*$^{-/-}$ mice was consistently within a similar range to that observed in *Cd4*$^{-/-}$ animals (Figure 5B and Figure 4A). Furthermore, this protective effect was not likely due to altered extravasation potency of gld-derived splenocytes as similar number of brain infiltrated CD4+ T cells were observed between MPTP-treated WT rec. Rag1$^{-/-}$ and gld rec. Rag1$^{-/-}$ animals (average number of CD4+ T cells in the SNpc ± SEM: 81.6 ± 22.5 and 95.5 ± 38.2, respectively. P = 0.55, Mann-Whitney test). Together, these results suggest that CD4^{+} T_H cell-mediated DN cell death requires the expression of a functional FasL, but not IFN-γ.

DISCUSSION

Mounting evidence support the notion that innate immunity significantly contributes to dopaminergic neurodegeneration in PD (1). By contrast, although altered cellular and humoral functions have been reported in the peripheral immune system of PD patients, the role of adaptive immunity in the pathogenesis of this disorder has remained much more elusive (5, 20). Among these peripheral immune changes, the significant increased ratio of $CD8^+$ T_C to $CD4^+$ T_H cells and IFN-γ-producing to IL-4-producing T cells suggests the existence of a disease-associated shift to a T_C1- and T_H1-type immune response which may reflect and/or contribute to the harmful brain inflammatory reaction (21). Nonetheless, a role for the cellular arm of the adaptive immune system in neurodegeneration is curbed by the fact that no clear demonstration of a prominent involvement of leukocytes at the site of neuronal injury has been provided in PD. In this study, we present evidence that peripheral T-cells migrate to and accumulate in the brain parenchyma during parkinsonism. Importantly, we have shown that $CD4^+$, but not $CD8^+$ T-cells, are deleterious to DNs, which suggests that the adaptive immune system may contribute to disease progression in PD.

It is now well established that the CNS is not only continuously monitored by T-cells (22) but also massively invaded by peripheral leukocytes in neuropathological circumstances (23). In agreement with the seminal but rather preliminary observation by McGeer and colleagues showing a substantial presence of $CD8^+$ T-cells in the brain from one PD case (7), we now provide strong quantitative evidence from a large number of individuals that both $CD8^+$ and $CD4^+$ T lymphocytes markedly accumulate in the SNpc of PD patients. Consistent with a previous report (9), we found that experimental lesion of the nigrostriatal

pathway in MPTP-intoxicated mice results in a similar brain accumulation of T-cells. Yet, brain accumulation of T-cells following MPTP intoxication was not restricted to the SNpc. Indeed, other catecholaminergic areas known to be moderately injured following MPTP-treatment (24) were also invaded albeit to a lower extend. This extravasation of lymphocyte is not likely to be a generalized non-specific leukocyte response: 1) other leukocyte subsets including B-cells and NK cells were not detected in the lesioned SNpc, 2) an increased occurrence of T-cells was not observed in non-lesioned brain areas suggesting that this process does not simply reflect an overall enhancement of lymphocyte patrolling. Altogether, these findings indicate that, as with the glial cell reaction previously described, T-cell brain infiltration in PD most certainly represents a secondary and highly regulated pathogenic event associated with neuronal cell death. Such a cellular and site-specific brain immune response is not likely to be caused by a massive disruption of the BBB, for which little evidence exists in PD (25, 26) and which remains controversial in MPTP-intoxicated mice (27, 28). We showed a widespread BBB leakage that occurred shortly (6 hours) after neurotoxin exposure and was rapidly resolved (by 12 hours after MPTP), well before lymphocytic invasion. Taken together, these findings argue that lymphocyte brain infiltration is not a passive phenomenon. Instead, molecular and cellular changes associated with neuronal injury are likely to regulate this site-specific brain recruitment of T-cells. Possible mechanisms may involve early microglial cell activation and innate neuroinflammatory processes which could modify the local microenvironment. In line with this, we found an up-regulated expression of the ICAM-1 adhesion molecule on both capillaries and glial cells, which may participate in the attachment of leukocytes to the vascular endothelium and their diapedesis (29). Interestingly, a similar ICAM-1 over-expression was recently described in both PD SN and MPTP-intoxicated monkeys (30).

Although the level of T cell brain accumulation was found to be higher in disease model than in PD patients, one has to consider that the human disease progresses over several decades whereas it only last one to two weeks in mouse model. Moreover, investigations performed on human postmortem tissue most often address late pathomechanisms and can not therefore predict the intensity of the lymphocyte infiltration process which might be greater during earlier stages of the disease. Given that incidental Lewy body disease is considered by some authors to be a presymptomatic form of PD (31), it might be valuable to explore such lymphocytic invasion in those patients. Finally, it is worth noting that the distribution of T cell accumulation within the SNpc from PD patients is much more heterogeneous than that in MPTP mice. Indeed, in few instances, as shown in Figure 1, infiltrating T cells in PD brains were found to be clustered around the few remaining pigmented DA neurons whereas they were virtually absent in advanced depigmented areas. Such distribution suggests that the number of T cell reaching the target neurons is conceivably substantial and strengthens their possible involvement in DA cell demise.

A major contribution of our study is the demonstration that brain infiltration of T-cells actively participates in DN degeneration. A decreased vulnerability of DNs to MPTP toxicity associated with the removal of mature T lymphocytes was achieved by two different genetic immune defects (*Rag1*$^{-/-}$ and *Tcrb*$^{-/-}$), thus supporting a role for the cellular arm of the adaptive immune system in experimental parkinsonism. Our results are in agreement with a recent study showing a similar neuropathological improvement in MPTP-intoxicated severe combined immunodeficient (SCID) mice (32). Notably, our data further reveal that different T-cell subsets do not contribute equally to DN cell death. Indeed, while the predominance of infiltrated CD8^{+} over CD4^{+} T-cells was consistently observed both in PD patients and MPTP-intoxicated mice, removal of the CD8^{+} T-cell subset in *Cd8a*$^{-/-}$ mice did

not mitigate MPTP injury. In sharp contrast, the T_H cell deficiency achieved in *Cd4*$^{-/-}$ mice conferred as much neuroprotection as in *Rag1*$^{-/-}$ and *Tcrb*$^{-/-}$ animals, suggesting that CD4$^+$ T-cells mediate most if not all the deleterious activity associated with the adaptive immune response.

Since infiltrated T-cells highly express ICAM-1 as well as Lymphocyte function-associated antigen-1 (LFA-1) and CD44 (9, 30), we believe that most of them could be recruited from an activated/memory population. A mechanism of peripheral leukocyte activation secondary to MPTP intoxication has recently been proposed (32). In this model, nitrotyrosine modification within α-synuclein (α-Syn) promotes an antigen-specific T-cell response in draining lymph nodes. After migrating into the injured brain areas, these antigen-specific T-cells could undergo further activation and promote microglial cell-dependent neurodegeneration through cytokine release. Although the differential contribution of CD8$^+$ versus CD4$^+$ T-cells in this deleterious immune response was not addressed by the authors, their prediction analysis of α-Syn-specific T-cell epitopes suggested a significant potential for CD4$^+$ T-cells of mice expressing IA^k or IA^b MHC class II molecules to respond to nitrated epitopes of α-Syn. These data, taken in conjunction with our present findings, support a model in which MPTP-induced brain antigen modification most likely generates a secondary and harmful T_H cell response contributing to DN degeneration.

Looking at the cytotoxic mechanism mediated by the CD4$^+$ T-cell response following nigrostriatal pathway injury, we found that T-cell expression of FasL but not IFN-γ was required. It has been shown that IFN-γ is critical in microglial-mediated loss of DNs in MPTP-intoxicated mice (18). Yet, using two different experimental approaches, i.e. total and cell-specific IFN-γ deletion, we were unable to show a major role of this pro-

inflammatory cytokine in DA cell demise. While the reason for such discrepancy is still not clear, a lack of IFN-γ expression in our disease model could not be incriminated. Indeed, in agreement with a previous report (33), we were able to detect a rise in IFN-γ following MPTP-induced nigrostriatal pathway injury. Whether different treatment protocols lead to distinct involvement of IFN-γ in disease models will need further clarifications.

The requirement of FasL in $CD4^+$ T cell-mediated cytotoxicity is consistent with the finding that Fas-deficient mice display attenuated MPTP-induced DN loss (34) although another study has come to a different conclusion (35). Whereas, in the context of antigen presentation, the Fas/FasL pathway has been implicated in the deletion of activated macrophages thereby contributing to the resolution of inflammation (36), recent evidence suggests that this pathway may instead induce proinflammatory cytokine responses in tissue macrophages (37). $CD4^+$ T_H FasL-mediated activation of microglial cells could therefore participate in the inflammatory reaction and DN degeneration. T-cell-derived FasL may also mediate inflammatory responses in astrocytes which are known to be particularly resistant to Fas-mediated cell death and express proinflammatory cytokines and chemokines upon Fas ligation (38). In line with this, Fas expression has been shown to be upregulated on these glial cells both in PD patients and in the MPTP model (34, 39). Alternatively, infiltrated $CD4^+$ T-cells may also induce DN cell demise through cell–cell contact. Such a mechanism has previously been evidenced *in vitro*, where antigen primed $CD4^+$ or $CD8^+$ T-cells induced neuronal death independently of antigen presentation and involving cell surface expression of FasL by activated T-cells (40). Further investigations will be required to determine whether or not $CD4^+$ T cell-mediated cytotoxicity relies strictly on MHC-dependent antigen presentation.

In our disease model, the finding that harmful lymphocyte response is CD4 T cell-dependent but IFN-γ-independent raises important but still unresolved concern about the phenotypic characteristics of these CD4 T cells. Although these observations would not favor the contribution of a T_H1-type response, one can not exclude the possibility that CD4+ T_H1 cells may mediate cytotoxicity independently of IFN-γ as previously reported (40, 41). In particular, the role of other proinflammatory T_H cytokines such as TNF-α in T cell-mediated DN cell death should also be considered as a potential deleterious mechanism even though the role of this factor is still debated (42-44). Finally, another tantalizing possibility could be the involvement of an alternative inflammatory CD4 T cell population namely the recently described T_H17 cells. A growing body of evidence indicates that T_H17 cells play a critical function not only in protection against microbial challenges but also in many organ-specific autoimmune diseases including multiple sclerosis and its disease model experimental autoimmune encephalomyelitis (45). In line with this, it has recently been shown that T_H17 cells have the potential of killing neurons probably through the granzyme B cytolytic enzyme system (46). Whether such CD4 T-cell subset is implicated in parkinsonism as well merits further considerations.

It is worth noting that the $CD4^+$ T cell response to neurodegenerative processes can differently affect disease outcome. Indeed, while in the MPTP mouse model of PD CD4+ T cells are likely harmful to DNs (present data and reference 32), it has recently been documented that this T cell population can provide supportive neuroprotection in animal model of inherited amyotrophic lateral sclerosis (ALS) by stimulating the trophic properties of glia (47). Interestingly, such pathological improvement can be recapitulated by delivering activated regulatory or effector T cells to ALS mice but not by Copolimer-1 immunization indicating that antigen-driving T_H2/T_H3 responses are impaired in this animal model (48).

Thus, different neurodegenerative contexts could result in distinct T cell responses which in turn may positively or negatively influence disease progression. Undoubtedly, a better phenotypic characterization of these CD4+ T cell subsets should improve our understanding on the role of the adaptive immune system in various neurodegenerative conditions.

In summary, we have shown that peripheral T-cells infiltrate the brain parenchyma at the site of neuronal injury both in PD patients and in experimental parkinsonism. We have demonstrated that this cell-mediated immune response contributes to DN cell degeneration through a $CD4^+$ T cell-dependent Fas/FasL cytotoxic pathway. Our results together with recent investigations (32) provide further rationales for targeting the adaptive arm of the immune system in PD. Therapeutic strategies may involve vaccination for antigens that promote cell-mediated anti-inflammatory responses (49, 50) as well as blocking the migration of immune cells across the BBB (51). Besides providing potential neuroprotective benefits for remaining DNs, these immunomodulatory strategies may also be of interest for cell transplantation therapies as long-term survival of grafted DNs, which eventually undergo PD-related pathological changes over time, could be jeopardize by such an immune-related hostile microenvironment (52).

METHODS

Human samples. The study was performed on autopsy brainstem tissue from 8 control subjects and 14 parkinsonian patients, well characterized clinically and neuropathologically. PD patients and control subjects did not differ significantly in terms of their mean age at death (mean ± s.e.m.: PD, 77.85 ± 2.11; controls, 76.62 ± 3.72 years: P = 0.76, Student's t test) or the mean interval from death to freezing of tissue (mean ± s.e.m.: PD, 40.55 ± 3.80; controls, 28.10 ± 7.08 hours; P = 0.11, Student's t test). Due to limited accessibility to tissue sections, different numbers of patient were analysed between leukocyte markers. Tissue was fixed in formaldehyde and then embedded in paraffin. Paraffin-embedded tissues were cut in serial 8-µm-thick slices on a microtome, and sections were recovered on SuperFrost Plus slides (Kindler O GmbH, Freiburg, Germany), before incubation at 56°C for 3 days. Human tonsil slices from Dako (Trappes, France) were used as tissue control for lymphoid marker immunohistochemistry.

Animals. Ten- to twelve-week-old male C57BL/6J mice, weighing 25–30 g, (CERJ, Le-Genest-St-Isle, France) were used. The following strains were obtained from Jackson Laboratories (Bar Harbor, ME): B6.129S6-*Cd4*^{tm1Knw}/J, B6.129S2-*Cd8a*^{tm1Mak}/J, B6.129P2-*Tcrb*^{tm1Mom}/J, B6.129S7-Rag1^{tm1Mom}/J, B6.129S7-Ifng^{tm1Ts}/J, B6Smn.C3-Faslgld/J and corresponding parental wild-type inbred C57BL/6J. Mice were kept in a temperature-controlled room (23° ± 1°C) under a 12-h light/dark cycle and had *ad libitum* access to food and water. All animals were further genotyped after their sacrifice according to Jackson Laboratories protocols. GFP$^+$ cells were isolated from double Tie2-Cre$^+$/ZEG$^+$ transgenic mice (designated GFP-Tg) in which the GFP reporter gene is expressed in early

hematopoietic cell precursors (53). Animal handling was carried out according to ethical regulations and guidelines contained in the *Guide for the Care and Use of Laboratory Animals* (National Research Council 1996) and the European Communities Council Directive 86/609/EEC.

Treatment and tissue preparation. Groups of mice received four i.p. injections of MPTP-HCl (20 mg/kg, except where otherwise stated) at 2 h intervals and were sacrificed from 6 hours to 21 days after the last injection. Control mice received saline solution only. For immunohistochemistry, mice were euthanized with 100 mg/kg pentobarbital, and transcardially perfused first with 50 ml of heparin solution (5U/ml) then with 100 ml of 4% paraformaldehyde. Brain and spleen free-floating sections were prepared as described elsewhere (54). For HPLC analysis of MPP^+ levels, brains were rapidly removed from the skull and striata dissected on humidified filters at 4°C. Tissues were then immersed in appropriate buffer.

Passive transfers. Single-cell suspensions were prepared from spleen and/or lymph nodes isolated from either Tie2-Cre^+/ZEG^+, *gld*, *Ifn-*$\gamma^{-/-}$ or C57BL/6J mice. GFP^+ T- and B-cells were purified with a cell magnetic separator (MACS, Miltenyi Biotech, CA) according to the manufacturer's procedure using anti-TCRβ (H57-597), anti-CD3ε (145-2C11), anti-CD4 (H-129.19), anti-CD8α (53-6.7) and anti-B220 conjugated PE antibodies (Pharmingen) and anti-PE-conjugated MicroBeads. Cells labeled with MicroBeads were retained on the MACS Column while unlabeled cells passed through. The column was removed from the seperator and the retained cells were eluted as the enriched, positively selected cell fraction. The enrichment of cells was confirmed by flow cytometry analysis using a FACS-

Calibur (e.g. more than 95% for T-cells, Supplemental Figure 2A). Recipient *Rag1*$^{-/-}$ mice received a single i.v. injection of either 10^7 GFP$^+$ T-cells or 2.5 10^7 GFP$^+$ B-cells, or 2 injections, 4 h apart, of 10^7 total splenocytes (either *gld*, *Ifn-γ*$^{-/-}$ or WT) in 0.2 ml phosphate buffered saline solution. Reconstitutions of GFP-expressing T and B lymphocytes in *Rag1*$^{-/-}$ recipient mice were checked by fluorescence-activated cell-sorter (FACS) analysis of blood samples collected from reconstituted *Rag1*$^{-/-}$ recipient mice prior to MPTP treatment or from lymph nodes after their sacrifice (Supplemental Figure 2C). Three to four weeks after transfer, mice were intoxicated with MPTP or received an equal volume of saline solution.

Immunohistochemistry. Human sections were first deparaffinized in 2 changes of xylene for 5 min each. They were hydrated in two changes of 100%, 95% then 75% ethanol and rinsed in distilled water. Antigen demasking was performed at 90–95°C for 30 min in citrate buffer pH=6 (for CD8, CD20, CD79a and CD57 staining) or EDTA buffer pH=8 for CD4 staining. Sections were then allowed to cool down for 20 min before being rinsed in 0.25 M Tris buffer.

Human sections were pretreated with 0.01% H_2O_2/20% methanol, followed by 0.5% Triton and by normal goat serum (1/30, 30 min). They were then incubated at 4°C for 48 h with anti-CD8 (1/50, Dako), anti-CD4 (1/20, Novo Castra, Newcastle, UK), anti-CD79α (1/100, Novo Castra), anti-CD20 (1/100, L26, Novo Castra) or anti-CD57 (1/50, Zymed, South San Francisco, CA).

Immunohistochemical staining on mouse brain sections was performed as previously described (51). The following primary antibodies were used: anti-TH (1/1000, Peel Freez Biochemicals, Rogers, AR), anti-Mac-1/CD11b (1/250, Serotec, Raleigh, NC), anti-GFAP (astrocytes, 1/5000, Dako), anti-GFP (1/1000, Invitrogen-Molecular Probes, Cergy

Pontoise, France), anti-CD3 (1/1000, Serotec), anti-CD8 (1/100, Serotec) or anti-CD4 (1/100, Serotec). Staining was revealed by the ABC method (Vector Laboratories, Burlingame, CA) with 3,3′-diaminobenzidine as the peroxidase substrate. Mouse sections were counterstained with thionin solution (Nissl stain) whereas human sections were counterstained with hematoxylin-and-eosin solution.

For double-staining experiments, brain sections were simultaneously incubated with two primary antibodies developed in different species: anti-tyrosine hydroxylase (1/1000, Peel Freez Biochemicals), anti-GFP (1/1000, Molecular Probes), anti Glut-1 (1/300, Santa Cruz Biotechnology, CA), anti-PCNA (1/500, Dako), anti-Mac-1 (1/250, Serotec), anti-GFAP (1/5000, Dako), anti-CD3 (1/1000, Serotec), anti-CD8 (1/100, Serotec), anti-CD4 (1/100, Serotec), anti-ICAM-1 (1/50, Serotec), anti-albumin (1/1000, Cappel - MP Biomedicals, Strasbourg, France) and anti-p17 Caspase3 (R&D systems). Sections were then incubated in specific CY3- or FITC-conjugated secondary antibodies (Jackson ImmunoResearch Laboratories) at 1/250 dilution for 90 minutes at room temperature (RT). For PCNA staining, sections were pretreated in 30% ethanol for 2 minutes and 70% ethanol at -20°C for 20 minutes. Hoechst nuclear staining was performed as previously described (53).

Electron microscopy. Ultrastructural analysis of T-cells in the SNpc was performed as previously described with minor modifications (55). In brief, small blocks of mesencephalon containing the SNpc were fixed in a mixture of 4% paraformaldehyde and 2.5% glutaraldehyde. Sections 50 µm thick were cut and labeled for CD8 as described above. Following identification of $CD8^+$ cells, small areas of sections were then excised and post-fixed in 1% osmium tetroxide for 30 min, rinsed in distilled water, dehydrated in a graded series of ethanol solutions, and embedded in Epon. Ultrathin (70 nm) sections were cut,

counterstained with conventional techniques and analysed with a JEOL 1200EX II electron microscope at 80 kV.

Measurement of striatal dopamine. Striatal levels of dopamine and its metabolites (DOPAC, HVA) were determined by high-performance liquid chromatography (HPLC) as previously reported (42).

Measurement of striatal MPP^+. Mice were killed 90 min after one i.p. injection of 30 mg/kg MPTP-HCl, and their striata were recovered and processed for HPLC using UV detection (295-nm wavelength) to measure MPP^+, as described elsewhere (56).

Antibody array. C57BL/6J mice (*n* = 5 per group) were intoxicated with MPTP and sacrificed from 12 hours to 7 days after the last injection. Controls received an equal volume of saline solution. The expression level of various cytokines in protein homogenates prepared from the ventral mesencephalon was analysed using a mouse antibody array glass chip (RayBio® Mouse Cytokine Antibody Array G series 1000, RayBiotech Inc). Incubation, washes, and exposure to film were done according to the manufacturer's instructions. Briefly, chip arrays were blocked at RT for 30 min before being incubated with 50-100 µl of each sample at RT for 2 h. Glass chips were then washed and incubated with biotin-conjugated primary antibody and Alexa Flour 555-conjugated streptavidin according to the manufacturer's instructions. Fluorescence detection and analysis were performed using an Axon GenePix laser scanner.

Image and data analysis. DAB-immunostained sections were analysed by bright field microscopy using a Leitz microscope equipped with image analysis software (Mercator, ExploraNova, La Rochelle, France). TH^+ and $Nissl^+$ cell bodies were quantified stereologically on regularly spaced sections covering the whole SNpc using the VisioScan stereology tool. The investigator performing the quantification was blinded to the treatment and genotype groups during the analysis. Fluorescent sections were analysed on a Zeiss Axioplan 2 using ExploraNova FluoUp 1.0 software.

Statistical analysis. All values are expressed as the mean ± SEM. Differences among means between two groups were analyzed using Student's *t* test or, when data were not normally distributed, with a non-parametric Mann-Whitney test. Differences among means between multiple data sets were analyzed using one- or two-way ANOVA with time, treatment or genotype as the independent factors. When ANOVA showed significant differences, pair-wise comparisons between means were tested by Tukey *post hoc* analysis. When data were not normally distributed, ANOVA on ranks was used (Kruskal-Wallis test followed by pairwise comparison using Dunn's method). In all analyses, the null hypothesis was rejected at the 0.05 level (SigmaStat Statistical Software, Jendel, St. Raphael, CA).

ACKNOWLEDGMENTS

We thank Drs. C. Combadière and C. Lobsiger for helpful discussions, Dr. V. Sazdovitch for assistance in collecting *postmortem* material and Dr. T. Welte for providing Tie2-Cre^{+}/ZEG^{+} double transgenic mice. This work was supported by grants from The Michael J. Fox Foundation (SH and ECH), Fondation pour la Recherche sur le Cerveau (SH), Fondation France Parkinson (VB) and the German Academic Exchange Service (DA-F). RAF is an investigator at the Howard Hughes Medical Institute. ECH and SH are investigators at the Centre National de la Recherche Scientifique (CNRS).

REFERENCES

1. Dauer, W. and Przedborski, S. 2003. Parkinson's disease: mechanisms and models. *Neuron* **39**: 889-909.
2. Chen, H. et al. 2005. Nonsteroidal antiinflammatory drug use and the risk for Parkinson's disease. *Ann. Neurol.* **58**: 963-967.
3. Wahner, A.D., Bronstein, J.M., Bordelon, Y.M. and Ritz, B. 2007. Nonsteroidal anti-inflammatory drugs may protect against Parkinson disease. *Neurology* **69**: 1836-1842.
4. Nagatsu, T., Mogi, M., Ichinose, H. and Togari, A. 2000. Changes in cytokines and neurotrophins in Parkinson's disease. *J. Neural Transm. Suppl.* **60**: 277-290.
5. Czlonkowska, A., Kurkowska-Jastrzebska, I., Czlonkowski, A., Peter, D. and Stefano, G.B. 2002. Immune processes in the pathogenesis of Parkinson's disease – a potential role for microglia and nitric oxide. *Med. Sci. Monit.* **8**: 165-177.
6. Whitton, P.S. 2007. Inflammation as a causative factor in the aetiology of Parkinson's disease. *Br. J. Pharmacol.* **150**: 963-976.
7. McGeer, P.L., Itagaki, S., Akiyama, H. and McGeer, E.G. 1988. Rate of cell death in parkinsonism indicates active neuropathological process. *Ann. Neurol.* **24**: 574-576.
8. Hunot, S. et al. 1999. FcεRII/CD23 is expressed in Parkinson's disease and induces, in vitro, production of nitric oxide and tumor necrosis factor-α in glial cells. *J. Neurosci.* **19**: 3440-3447.
9. Kurkowska-Jastrzebska, I., Wrońska, A., Kohutnicka, M., Czlonkowski, A. and Czlonkowska, A. 1999. The inflammatory reaction following 1-methyl-4-phenyl-1,2,3, 6-tetrahydropyridine intoxication in mouse. *Exp. Neurol.* **156**: 50-61.

10. Janeway Jr, C.A. and Travers, P. 1997. *Immunobiology: the immune system in health and disease*. Current Biology Ltd/Garlan Publishing Inc, London/New York, UK/USA.

11. Kortekaas, R. et al. 2005. Blood-brain barrier dysfunction in parkinsonian midbrain in vivo. *Ann. Neurol.* **57**: 176-179.

12. Engelhardt, B. 2006. Molecular mechanisms involved in T cell migration across the blood-brain barrier. *J. Neural Transm.* **113**: 477-485.

13. Serpe, C.J., Kohm, A.P., Huppenbauer, C.B., Sanders, V.M. and Jones, K.J. 1999. Exacerbation of facial motoneuron loss after facial nerve transection in severe combined immunodeficient (*scid*) mice. *J. Neurosci.* **19**: RC7, 1-5.

14. Chen, Z., Ljunggren, H.G., Zhu, S.W., Winblad, B. and Zhu, J. 2004. Reduced susceptibility to kainic acid-induced excitotoxicity in T-cell deficient CD4/CD8 (-/-) and middle-aged C57BL/6 mice. *J. Neuroimmunol.* **146**: 33-38.

15. Mombaerts, P. et al. 1992. Mutations in T-cell antigen receptor genes alpha and beta block thymocyte development at different stages. *Nature* **360**: 225-231.

16. Fung-Leung, W.P. et al. 1991. CD8 is needed for development of cytotoxic T-cells but not helper T-cells. *Cell* **65**: 443-449.

17. Rahemtulla, A. et al. 1991. Normal development and function of CD8+ cells but markedly decreased helper cell activity in mice lacking CD4. *Nature* **353**: 180-184.

18. Mount, M.P. et al. 2007. Involvement of interferon-γ in microglial-mediated loss of dopaminergic neurons. *J. Neurosci.* **27**: 3328-3337.

19. Takahashi, T. et al. 1994. Generalized lymphoproliferative disease in mice, caused by a point mutation in the Fas ligand. *Cell* **76**: 969-976.

20. Hunot, S. and Hirsch, E.C. 2003. Neuroinflammatory processes in Parkinson's disease. *Ann. Neurol.* **53** (suppl 3): S49-S60.

21. Baba, Y., Kuroiwa, A., Uitti, R.G., Wszolek, Z.K. and Yamada, T. 2005. Alterations of T-lymphocyte populations in Parkinson disease. *Parkinsonism Relat. Disord.* **11**: 493-498.

22. Cose, S., Brammer, C., Khanna, K.M., Masopust, D. and Lefrançois, L. 2006. Evidence that a significant number of naive T cells enter non-lymphoid organs as part of a normal migratory pathway. *Eur J Immunol.* **36**: 1423-33.

23. Togo, T. et al. 2002. Occurrence of T cells in the brain of Alzheimer's disease and other neurological diseases. *J. Neuroimmunol.* **124**: 83-92.

24. German, D.C. et al. 1996. The neurotoxin MPTP causes degeneration of specific nucleus A8, A9 and A10 dopaminergic neurons in the mouse. Neurodegeneration **5**: 299-312.

25. Farkas, E., De Jong, G.I., de Vos, R.A., Jansen Steur, E.N. and Luiten, P.G. 2000. Pathological features of cerebral cortical capillaries are double in Alzheimer's disease and Parkinson's disease. *Acta Neuropathol.* **100**: 395-402.

26. Haussermann, P., Kuhn, W., Przuntek, H. and Muller, T. 2001. Integrity of the blood-cerebrospinal fluid barrier in early Parkinson's disease. *Neurosci. Lett.* **300**: 182-184.

27. Adams, J.D. Jr, Klaidman, L.K., Odunze, I.N. and Johannenssen, J.N. 1991. Effects of MPTP on the cerebrovasculature. *Int. J. Dev. Neurosci.* **9**: 155-159.

28. Zhao, C., Ling, Z., Newman, M.B., Bhatia, A. and Carvey, P.M. 2007. TNF-α knockout and minocycline treatment attenuates blood-brain barrier leakage in MPTP-treated mice. *Neurobiol. Dis.* **26**: 36-46.

29. Springer, T.A. 1994. Traffic signals for lymphocyte recirculation and leukocyte emigration: the multistep paradigm. *Cell* **76**: 301-314.

30. Miklossy, J. et al. 2005. Role of ICAM-1 in persisting inflammation in Parkinson disease and MPTP monkeys. *Exp. Neurol.* **197**: 275-283.

31. Jenner, P. and Olanow, C. W. 1998. Understanding cell death in Parkinson's disease. *Ann. Neurol.* **44, Suppl. 1**: 72-84.

32. Benner, E.J. et al. 2008. Nitrated α-synuclein immunity accelerates degeneration of nigral dopaminergic neurons. *PloS ONE* **3**: e1376.

33. Ciesielska, A. et al. 2003. Dynamics of expression of the mRNA for cytokines and inducible nitric synthase in a murine model of the Parkinson's disease. *Acta Neurobiol. Exp.* **63**: 117-126.

34. Hayley, S. et al. 2004. Regulation of dopaminergic loss by Fas in a 1-methyl-4-phenyl-1,2,3,6-tetrahydropyridine model of Parkinson's disease. *J. Neurosci.* **24**: 2045-2053.

35. Landau, A.M. et al. 2005. Defective Fas expression exacerbates neurotoxicity in a model of Parkinson's disease. *J Exp Med.* **202**: 575-581.

36. Ashany, D. et al. 1995. Th1 CD4+ lymphocytes delete activated macrophages through the Fas/APO-1 antigen pathway. *Proc. Natl. Acad. Sci. USA* **92**: 11225-11229.

37. Park, D.R. et al. 2003. Fas (CD95) induces proinflammatory cytokine responses by human monocytes and monocyte-derived macrophages. *J. Immunol.* **170**: 6209-6216.

38. Choi, C and Benveniste, E.N. 2004. Fas ligand/fas system in the brain : regulator of immune and apoptosis responses. *Brain Res. Rev.* **44**: 65-81.

39. Ferrer, I., Blanco, R., Cutillas, B. and Ambrosio, S. 2000. Fas and Fas-L expression in Huntington's disease and Parkinson's disease. *Neuropathol. Appl. Neurobiol.* **26**: 424-433.

40. Giuliani, F., Goodyer, C.G., Antel, J.P. and Yong, V.W. 2003. Vulnerability of human neurons to T cell-mediated cytotoxicity. *J. Immunol.* **171**: 368-379.

41. Ju, S.T., Cui, H., Panka, D.J., Ettinger, R. and Marshak-Rothstein, A. 1994. Participation of target Fas protein in apoptosis pathway induced by CD4+ Th1 and CD8+ cytotoxic T cells. *Proc. Natl. Acad. Sci. USA* **91**: 4185-4189.

42. Rousselet, E. et al. 2002. Role of TNF-alpha receptors in mice intoxicated with the parkinsonian toxin MPTP. *Exp Neurol.* **177**: 183-92.

43. Ferger, B., Leng, A., Mura, A., Hengerer, B. and Feldon, J. 2004. Genetic ablation of tumor necrosis factor-alpha (TNF-alpha) and pharmacological inhibition of TNF-synthesis attenuates MPTP toxicity in mouse striatum. *J Neurochem.* **89**: 822-33.

44. Sriram, K., Miller, D.B. and O'Callaghan, J.P. 2006. Minocycline attenuates microglial activation but fails to mitigate striatal dopaminergic neurotoxicity: role of tumor necrosis factor-alpha. *J Neurochem.* **96**: 706-718.

45. Zhu, J. and Paul, W.E. 2008. CD4 T cells: fates, functions, and faults. *Blood* **112**: 1557-1568.

46. Kebir, H. et al. 2007. Human Th17 lymphocytes promote blood-brain barrier disruption and central nervous system inflammation. *Nat. Med.* **13**: 1173-1175.

47. Beers, D.R., Henkel, J.S., Zhao, W., Wang, J. and Appel, S.H. 2008. CD4+ T cells support glial neuroprotection, slow disease progression, and modify glial morphology in an animal model of inherited ALS. *Proc. Natl. Acad. Sci. USA* **105**: 15558-1563.

48. Banerjee, R. et al. 2008. Adaptive immune neuroprotection in G93A-SOD1 amyotrophic lateral sclerosis mice. *PLoS ONE* **3**: e2740.

49. Benner, E.J. et al. 2004. Therapeutic immunization protects dopaminergic neurons in a mouse model of Parkinson's disease. *Proc. Natl. Acad. Sci. USA* **101**: 9435-9440.

50. Reynolds, A.D. et al. 2007. Neuroprotective activities of CD4+CD25+ regulatory T cells in an animal model of Parkinson's disease. *J. Leukoc. Biol.* **82**: 1083-1094.

51. Luster, A.D., Alon, R. and von Andrian, U.H. 2005. Immune cell migration in inflammation: present and future therapeutic targets. *Nat. Immunol.* **6**: 1182-1190.

52. Braak, H. and Del Tredici, K. 2008. Assessing fetal nerve cell grafts in Parkinson's disease. *Nat. Med.* **14**: 483-485.

53. Welte, T. et al. 2003. STAT3 deletion during hematopoiesis causes Crohn's disease-like pathogenesis and lethality: A critical role of STAT3 in innate immunity. *Proc. Natl. Acad. Sci. USA* **100**: 1879-1884.

54. Hunot, S. et al. 2004. JNK-mediated induction of cyclooxygenase 2 is required for neurodegeneration in a mouse model of Parkinson's disease. *Proc. Natl. Acad. Sci. USA* **101**: 665-670.

55. Hunot, S. et al. 1997. Nuclear translocation of NF-kappaB is increased in dopaminergic neurons of patients with Parkinson disease. *Proc. Natl. Acad. Sci. USA* **94**: 7531-7536.

56. Liberatore, G.T. et al. 1999. Inducible nitric oxide synthase stimulates dopaminergic neurodegeneration in the MPTP model of Parkinson disease. *Nat. Med.* **5**: 1403-1409.

FIGURE LEGENDS

Figure 1 Lymphocyte infiltration in PD brain. (**A**) CD8 and (**B**) CD4 immunostaining with hematein counterstain on mesencephalic transverse sections from PD patients. $CD8^+$ or $CD4^+$ T-cells (arrows) are found in close contact with blood vessels or have migrated deep into the brain parenchyma close to neuromelanin-containing DNs (arrowheads). Note that brain staining for CD79α and CD20 (B-cells), and CD57 (NK cells) was not detected in either group of patients. All antibodies were previously tested on human tonsil tissue sections taken as a positive control and all of them gave the expected cellular staining (Supplemental Figure 1) Scale bars: 250 µm, dashed boxes: 30 µm, Upper right panel in (b): 15 µm. (**C**) Ultrastructural view of an infiltrated $CD8^+$ T-cell in the SNpc from a parkinsonian patient. Parenchymal $CD8^+$ T-cells display a small cytoplasmic volume, membrane-type CD8 staining (arrowheads) and a uropod-like cytoplasmic extension usually involved in T-cell motility (arrow). Per, pericyte; BM, basal membrane; RBC, red blood cell; e, endothelial cell; m, mitochondria; n, nucleus. Scale bar: 4 µm. (**D**) Density of infiltrated $CD8^+$ (left) and $CD4^+$ T-cells (right) in the SNpc of parkinsonian patients (n = 14 and 9 for CD8 and CD4 staining, respectively) and age-matched control subjects (n = 4 and 7 for CD8 and CD4 staining, respectively). Bars represent the mean density. *, $P < 0.05$ and **, $P < 0.001$, compared with controls (Student's t test).

Figure 2 MPTP-induced nigrostriatal pathway injury stimulates T-cell brain infiltration in mouse. (**A**) Schematic representation of the experimental approach (see Methods). GFP^+ T-cell infiltration in the SNpc (**B**) and striatum (**C**) following MPTP intoxication. Numerous GFP^+ T-cells can be seen in the SNpc two days after MPTP but not saline exposure. GFP^+

T-cells are also found in the striatum from intoxicated mice, though are far fewer than in the SNpc. Scale bars: (B) 300 µm, (C) 100 µm (insets: 10 µm). (**D**) Immunofluorescent staining for TH, Glut1, CD8 or CD4. Note that infiltrated GFP^+ T-cells are clustered within the SNpc in close proximity to TH^+ DNs. Transmigrated GFP^+ T-cells are not found in the lumen of $Glut1^+$ blood vessels (arrows) and consist of both $CD8^+$ and $CD4^+$ T-cell subsets. Scale bars: 20 µm. (**E**) T-cell brain infiltration in MPTP-treated C57Bl/6 inbred mice. (Left) CD3 immunostaining showing numerous T lymphocytes within the SNpc (dashed line) from MPTP-treated mice. Scale bar: 100 µm. (Right) Kinetic of nigral $CD4^+$ and $CD8^+$ T-cell (insets) density after MPTP exposure. S: saline. Data points represent the mean ± SEM. *, $P < 0.01$, compared with saline- and MPTP-treated mice at day 4 after MPTP; †, $P < 0.01$, compared with saline-treated controls (Tukey *post hoc* analysis). Scale bars: 50 µm. (**F**) Double immunofluorescent staining for PCNA and GFP, GFAP or Mac1. Note that $PCNA^+$ cells in the SNpc never co-localize with GFP^+ or $GFAP^+$ cells whereas they superpose perfectly with $Mac\text{-}1^+$ macrophages/microglial cells (arrows). Scale bar: 50 µm.

Figure 3 Mechanism of lymphocyte entry into the brain. (**A**) Immunofluorescent staining for serum albumin on brain sections (forebrain and hindbrain levels are shown) from mice sacrificed 6 hours after the last MPTP or saline injection. Patches of staining (arrows) are detected in various brain areas at 6 hours following MPTP exposure but not after saline treatment. CTX: cortex, STR: striatum, RMC: magnocellular part of the red nucleus, VTA, ventral tegmental area, SNC, substantia nigra compacta, SNR: substantia nigra reticulata, Aq: aqueduct of Sylvius. Scale bar: 300 µm. (**B**) Immunostaining for CD54/ICAM-1 (red) on mesencephalic sections from MPTP-intoxicated GFP^+ T-cell-reconstituted $Rag^{-/-}$ mice. The expression pattern of CD54 overlaps with that of the GFP^+ T-cell infiltrate within the SNpc

(white dashed line). At higher magnification (right panel), CD54 expression is visible on GFP^+ T-cells (arrows), blood vessels (asterisks) and branched glial cells (arrowheads). Scale bars: 300 µm (left), 10 µm (right).

Figure 4 Mice deficient in $CD4^+$ T-cells are more resistant to MPTP. (**A**) Quantification of TH^+ DN neurons in the SNpc at day 7 after MPTP (4x18mg/kg) or saline treatment in WT, *Tcrb*$^{-/-}$, *Cd8a*$^{-/-}$ and *Cd4*$^{-/-}$ mice. Bars represent the mean number of total nigral TH^+ DNs. A significant protection against MPTP-induced DN cell loss is observed in *Tcrb*$^{-/-}$ and *Cd4*$^{-/-}$ mice, but not in *Cd8a*$^{-/-}$ animals as compared to their WT littermates. *, $P < 0.05$ compared with MPTP-treated WT and *Cd8a*$^{-/-}$ mice; †, $P = 0{,}956$ compared with MPTP-treated WT littermates (Tukey *post hoc* analysis). $Nissl^+$ cell counts confirmed that TH^+ cell loss was not a consequence of downregulated expression of TH (data not shown). (**B**) Representative photomicrographs of mesencephalic sections immunostained for TH with Nissl counterstain from saline- or MPTP-treated WT and lymphocytic deficient mice. Insets show Mac-1^+ microglial cells (arrows) in the SNpc from the same animals. Scale bar: 300 µm (inset: 100 µm). (**C**) Quantification of the total number of infiltrated $CD4^+$ and $CD8^+$ T-cells in the SNpc from MPTP-treated WT and lymphocytic deficient mice. MPTP-treated *Cd8a*$^{-/-}$ mice display as many $CD4^+$ T-cells as MPTP-treated WT littermates. *, $P < 0.05$ compared with saline-injected WT mice (Mann-Whitney test). †, $P < 0.001$ compared with MPTP-treated WT and *Cd8a*$^{-/-}$ mice; #, $P < 0.001$ compared with MPTP-treated WT mice (Dunn's pairwise comparison). n.d., not detected.

Figure 5 FasL, but not IFN-γ, is required T cell-mediated DN toxicity in MPTP mouse. (**A**) Quantification of TH^+ DNs in the SNpc at day 7 after MPTP (4x18mg/kg) or saline

treatment in WT and *Rag1*$^{-/-}$ mice reconstituted with spleen cells from either C57Bl/6 inbred or *Ifnγ*$^{-/-}$ donors. All groups of animals are equally sensitive to MPTP-induced DN injury. *, $P < 0.05$ compared with their saline counterparts; †, $P < 0.05$ compared with their saline counterparts but not different from MPTP-treated WT mice (Tukey *post hoc* analysis). (**B**) Quantification of TH^{+} DNs in the SNpc at day 7 after MPTP (4x18mg/kg) or saline treatment in non-reconstituted *Rag1*$^{-/-}$ mice (non rec. *Rag1*$^{-/-}$) and in *Rag1*$^{-/-}$ mice reconstituted with spleen cells from either C57Bl/6 or *gld* donors (WT rec. *Rag1*$^{-/-}$ and *gld* rec. *Rag1*$^{-/-}$, respectively). Non-reconstituted *Rag1*$^{-/-}$ mice and *gld* rec. *Rag1*$^{-/-}$ mice are partially protected against MPTP-induced DN loss as compared to WT rec. *Rag1*$^{-/-}$ animals. *, $P < 0.01$ compared to MPTP-intoxicated WT rec. *Rag1*$^{-/-}$ mice (Tukey *post hoc* analysis) (**C**) Representative photomicrographs of mesencephalic sections immunostained for TH with Nissl counterstain from saline- or MPTP-treated WT rec. *Rag1*$^{-/-}$ and *gld* rec. *Rag1*$^{-/-}$ mice. Scale bar: 300 µm.

Table 1

Striatal monoamine levels (pM/mg tissue)

	Dopamine	DOPAC	HVA
Saline			
Wild-type (*n*=5)	82.3 ± 7.5	15.4 ± 1.9	10.1 ± 1.0
Tcrb$^{-/-}$ (*n*=3)	85.4 ± 12.7	15.8 ± 3.0	9.5 ± 1.6
Cd8a$^{-/-}$ (*n*=3)	84.6 ± 4.1	16.0 ± 1.0	9.9 ± 0.9
Cd4$^{-/-}$ (*n*=3)	65.0 ± 8.9	15.7 ± 2.3	8.7 ± 1.4
MPTP			
Wild-type (*n*=5)	1.7 ± 0.3	1.8 ± 0.2	3.2 ± 0.4
Tcrb$^{-/-}$ (*n*=4)	2.8 ± 0.4	2.5 ± 0.3	3.7 ± 0.5
Cd8a$^{-/-}$ (*n*=4)	4.9 ± 1.6	2.2 ± 0.3	3.2 ± 0.1
Cd4$^{-/-}$ (*n*=4)	3.5 ± 0.5	3.0 ± 0.5	4.5 ± 0.6

Striatal dopamine, DOPAC and HVA levels in wild-type, *Tcrb*$^{-/-}$, *Cd8a*$^{-/-}$ and *Cd4*$^{-/-}$ mice at 7 days after the last MPTP injection do not differ ($P > 0.05$; Kruskal-Wallis test) between groups. Data represent means ± SEM for the indicated number of mice.

Table 2

Striatal MPP^+ levels (ng/mg tissue)

Wild-type	7.09 ± 2.95
Tcrb$^{-/-}$	6.00 ± 2.55
Cd8a$^{-/-}$	7.89 ± 2.17
Cd4$^{-/-}$	5.29 ± 2.16

Striatal MPP+ levels in wild-type, *Tcrb*$^{-/-}$, *Cd8a*$^{-/-}$ and *Cd4*$^{-/-}$ mice at 90 min after a single MPTP injection do not differ (P = 0.87; Kruskal-Wallis test) between groups. Data represent means ± SEM for five mice per group.

Figure 1

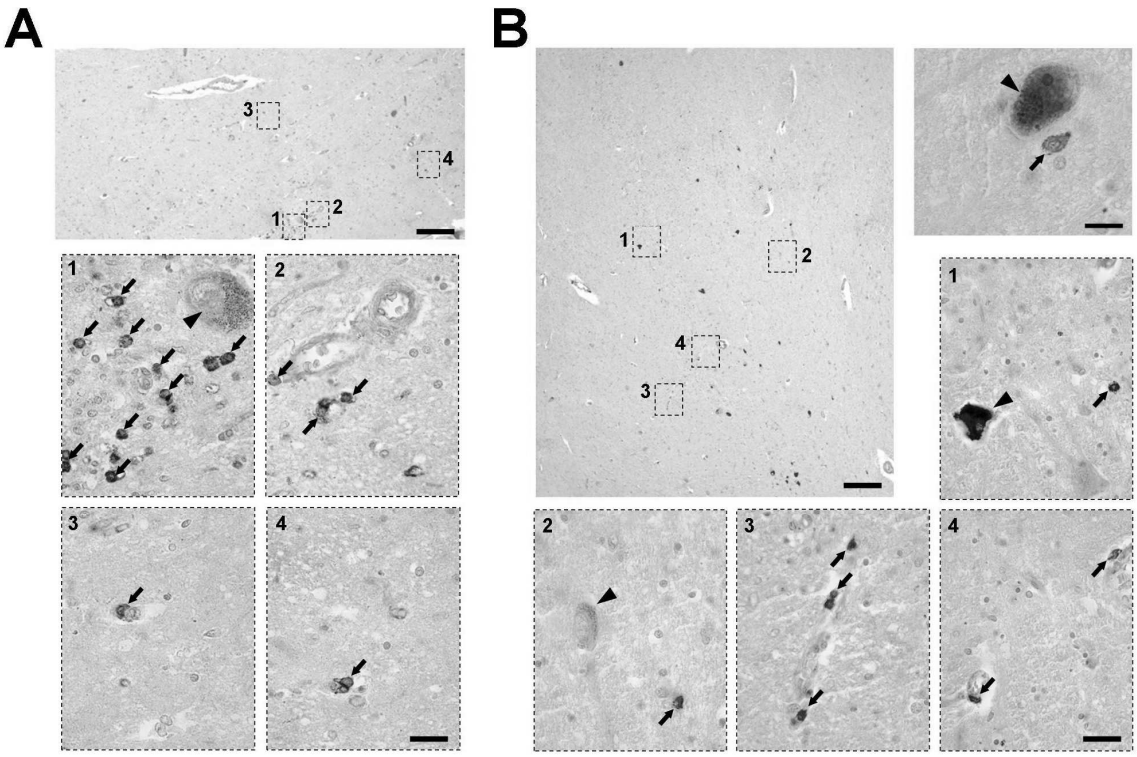
A
B
1
2
3
4

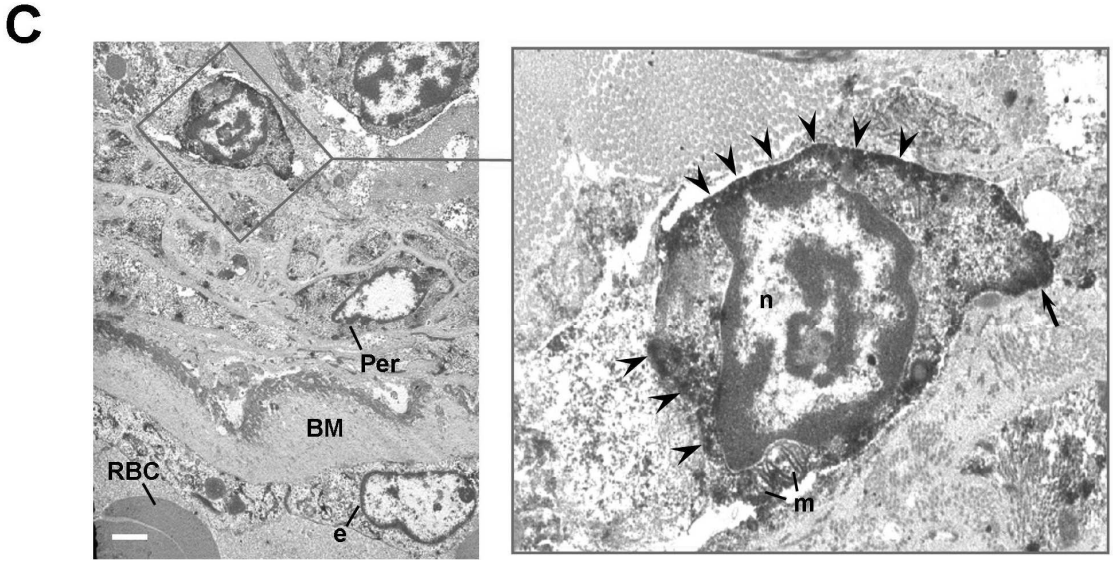
C
Per
BM
RBC
e
n
m

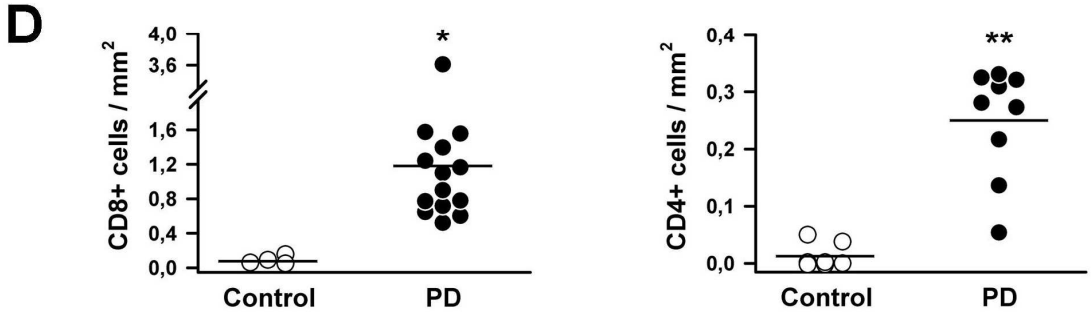
D
CD8+ cells / mm2
4,0
3,6
1,6
1,2
0,8
0,4
0,0
*
Control
PD
CD4+ cells / mm2
0,4
0,3
0,2
0,1
0,0
**
Control
PD

Figure 2

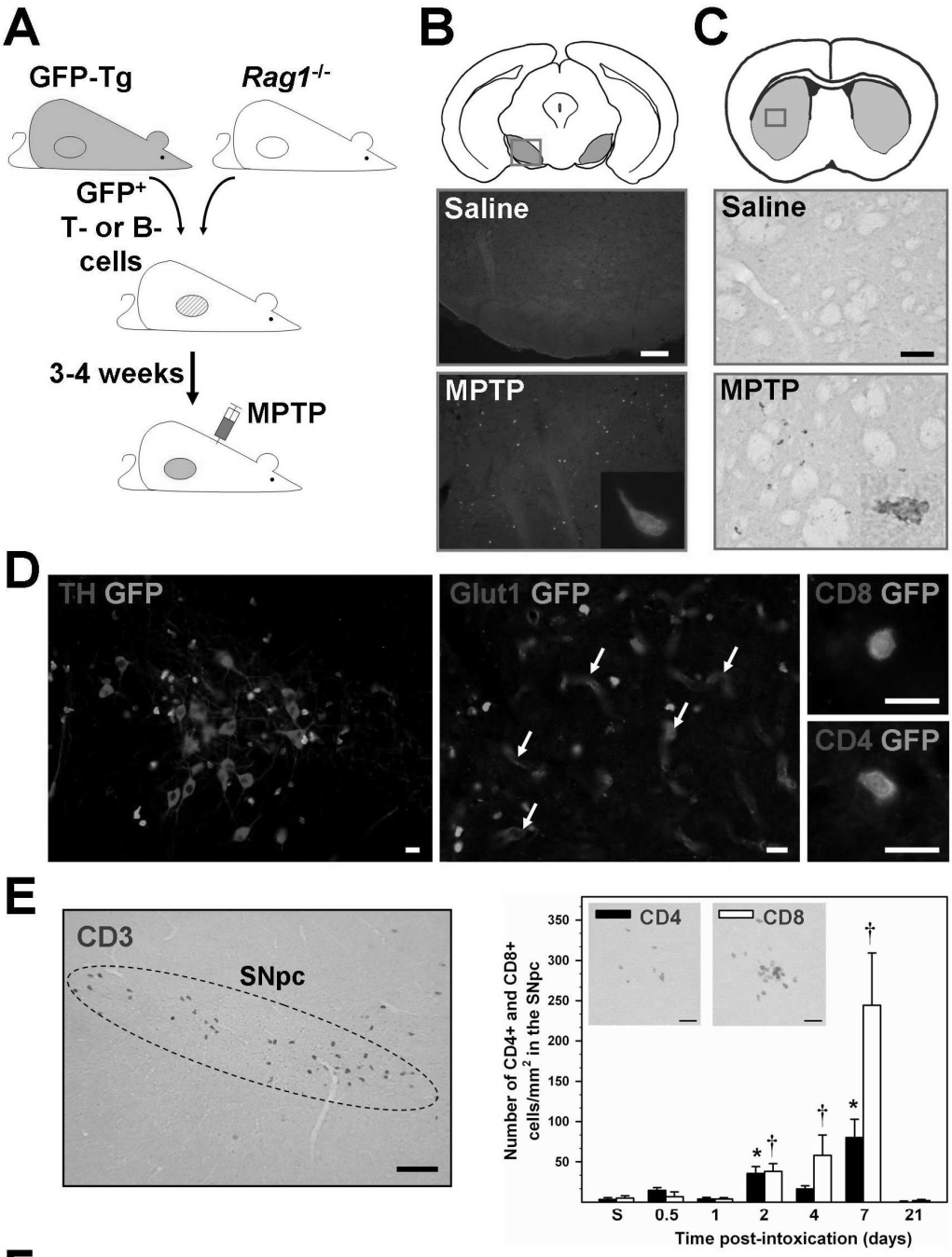
A
GFP-Tg
Rag1-/-
GFP+
T- or B-
cells
3-4 weeks
MPTP
B
C
Saline
Saline
MPTP
MPTP
D
TH GFP
Glut1 GFP
CD8 GFP
CD4 GFP
E
CD3
SNpc
CD4
CD8
Number of CD4+ and CD8+ cells/mm2 in the SNpc
350
300
250
200
150
100
50
S
0.5
1
2
4
7
21
Time post-intoxication (days)
F
PCNA GFP
PCNA GFAP
PCNA Mac1

Figure 3

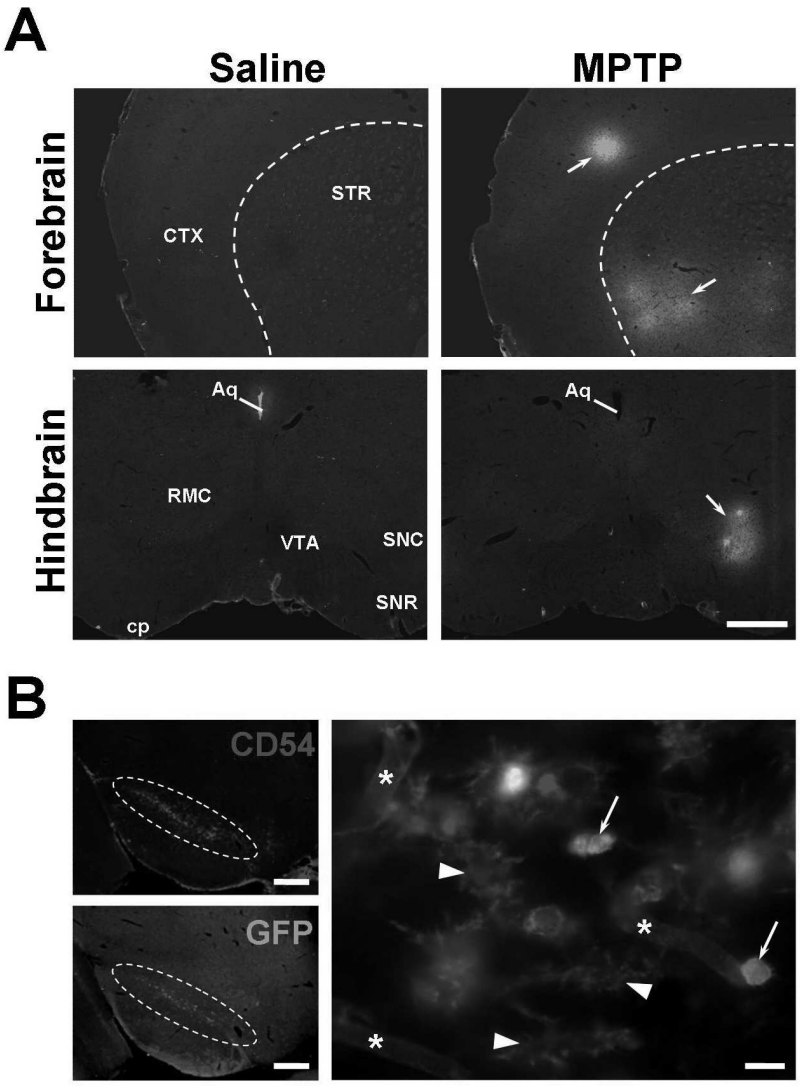
A
Saline
MPTP
Forebrain
STR
CTX
Hindbrain
Aq
RMC
VTA
SNC
SNR
cp
B
CD54
GFP

Figure 4

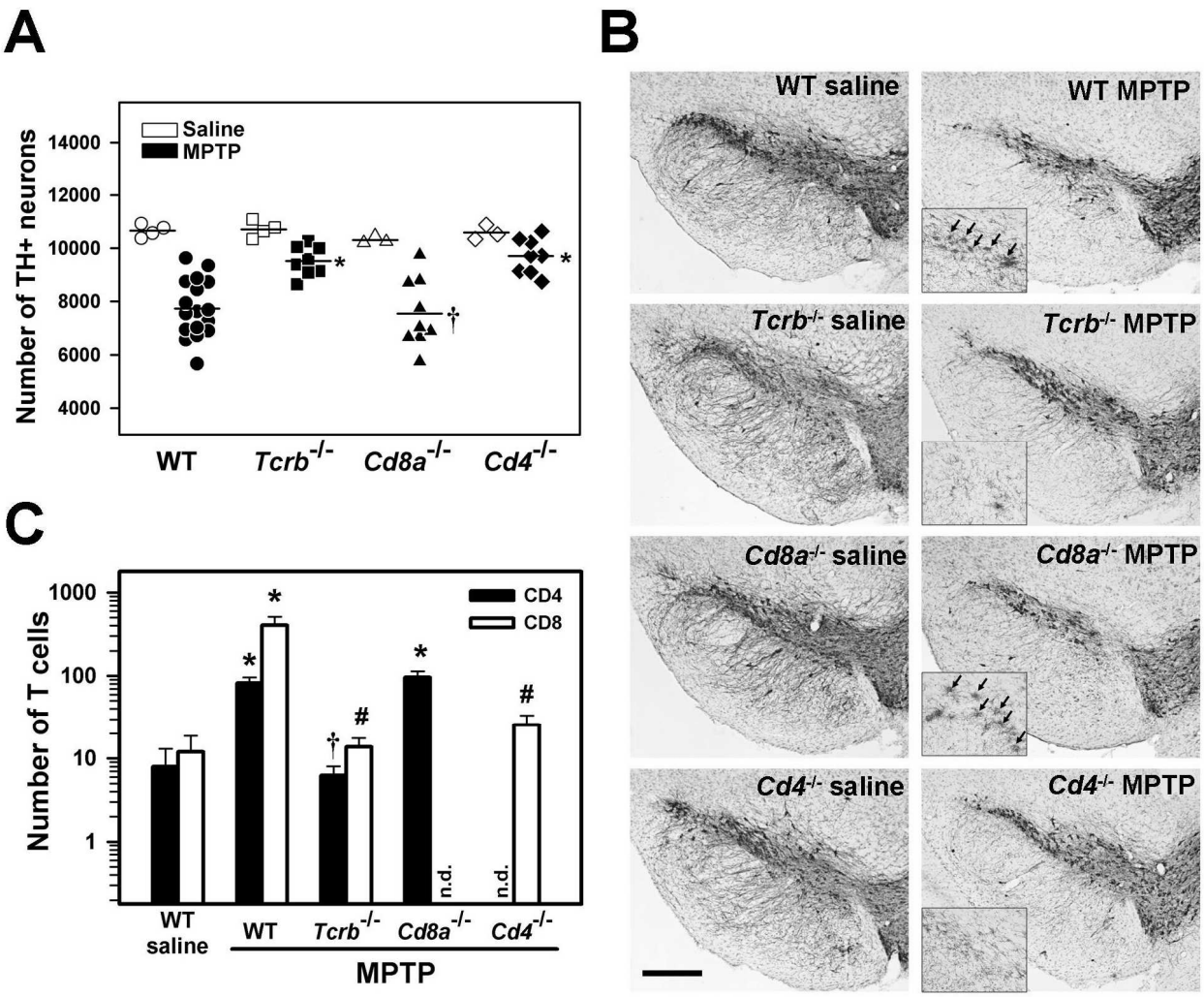
A
Saline
MPTP
Number of TH+ neurons
14000
12000
10000
8000
6000
4000
WT
Tcrb-/-
Cd8a-/-
Cd4-/-
B
WT saline
WT MPTP
Tcrb-/- saline
Tcrb-/- MPTP
Cd8a-/- saline
Cd8a-/- MPTP
Cd4-/- saline
Cd4-/- MPTP
C
CD4
CD8
Number of T cells
1000
100
10
1
n.d.
n.d.
WT saline
WT
Tcrb-/-
Cd8a-/-
Cd4-/-
MPTP

Figure 5

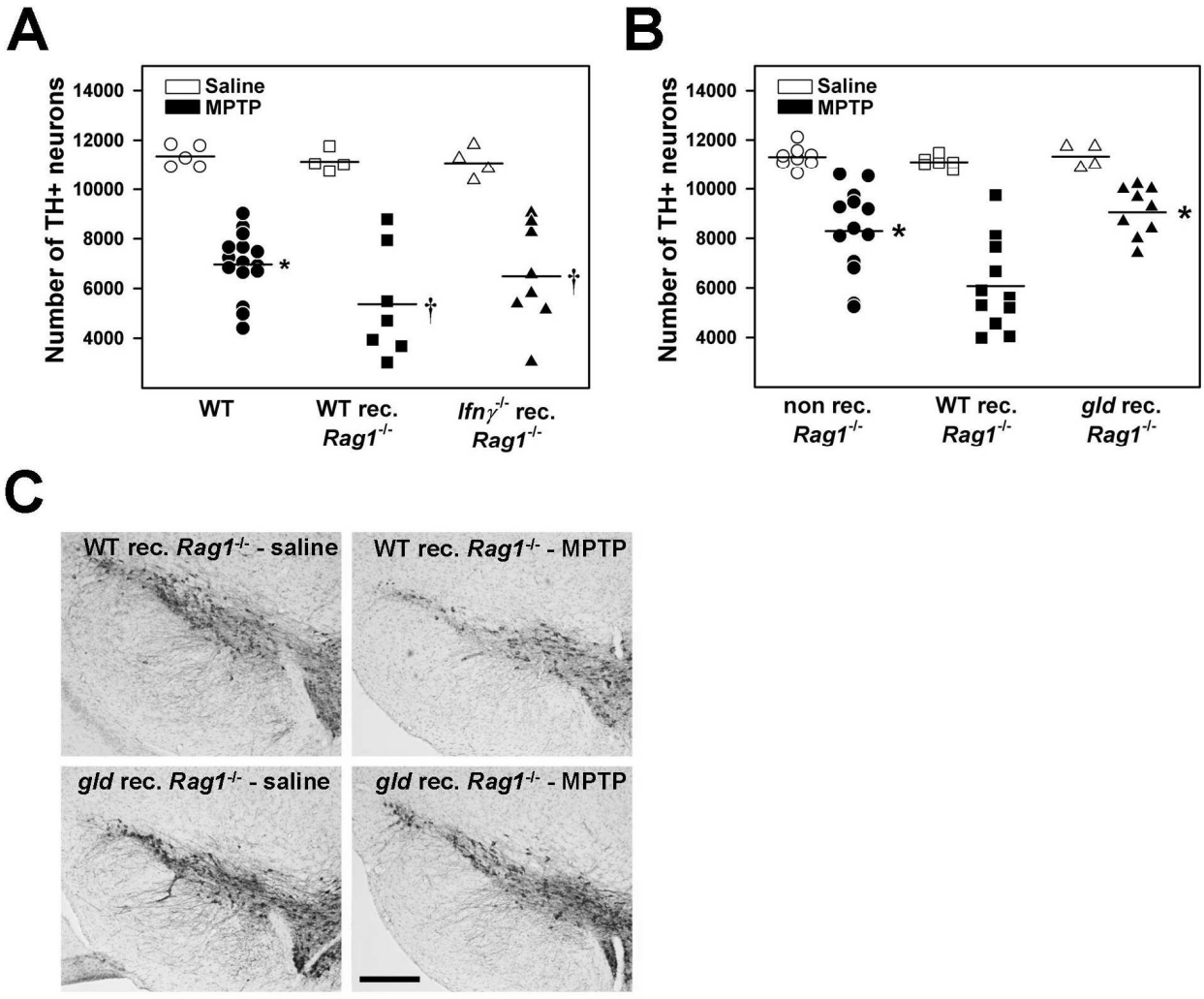
A
B
C
Saline
MPTP
Number of TH+ neurons
14000
12000
10000
8000
6000
4000
WT
WT rec. Rag1-/-
Ifnγ-/- rec. Rag1-/-
non rec. Rag1-/-
gld rec. Rag1-/-
WT rec. Rag1-/- - saline
WT rec. Rag1-/- - MPTP
gld rec. Rag1-/- - saline
gld rec. Rag1-/- - MPTP

Supplemental Table 1

Antibodies used for the detection of leukocyte subsets in the human brain

Antigen	Cellular expression	Function
CD8	Thymocyte subsets, cytotoxic T-cells	co-receptor for MHC class I
CD4	Thymocyte subsets, helper and inflammatory T-cells	co-receptor for MHC class II
CD79α	B-cells	component of the B-cell receptor complex
CD20	B-cells	putative calcium channel
CD57	natural killer cell	human lymphocyte oligosaccharide antigen

Supplemental Table 2

T-cell density in the red nucleus (cells/mm^2)

	Controls	PD
CD8$^+$	0.245 ± 0.040	0.155 ± 0.090
CD4$^+$	0.021 ± 0.014	0.009 ± 0.005

CD8$^+$ and CD4$^+$ T-cell density in controls and PD patients do not differ (P = 0.34 and P = 0.71, respectively; Student's t test). Data represent means ± SEM

Supplemental Figure 1

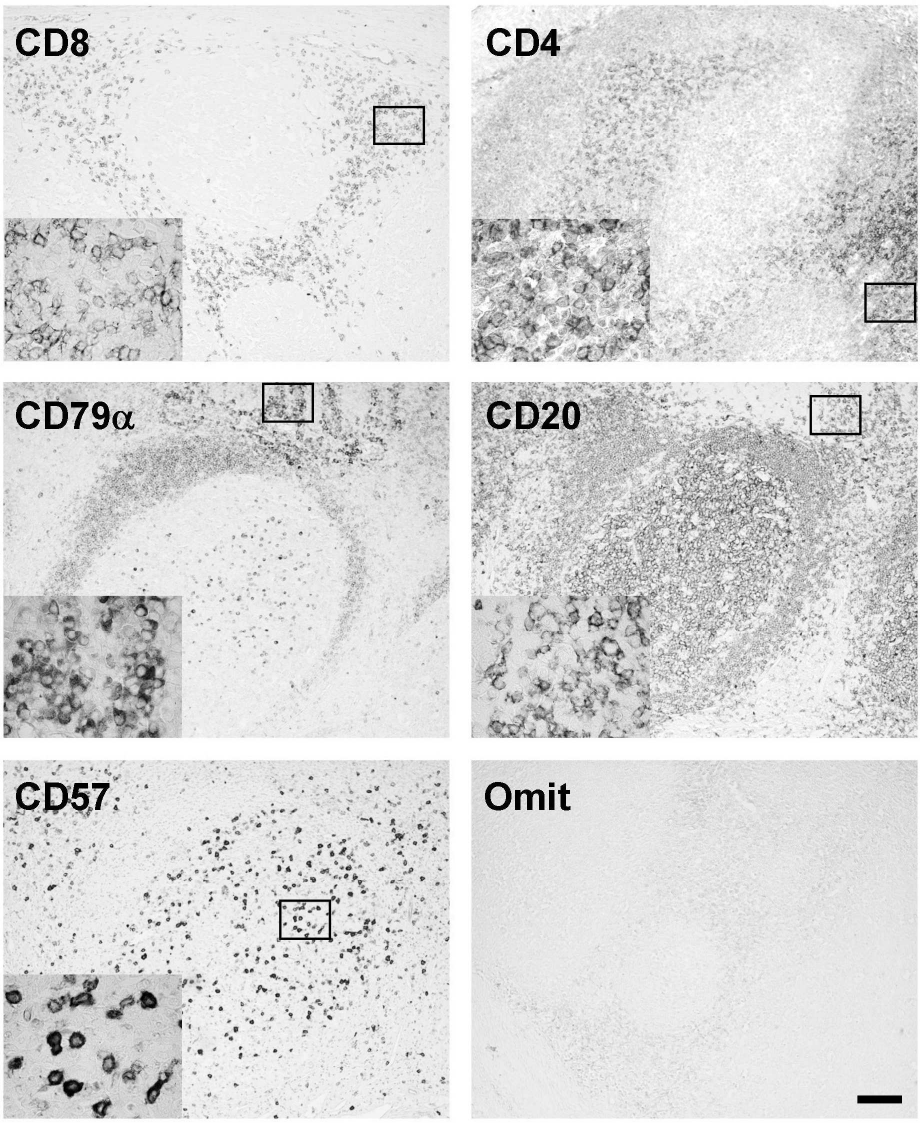

Supplemental Figure 1: Immunohistochemical detection of leukocyte subsets in human tonsil control tissue. Representative photomicrographs of human tonsil tissue sections immunostained for either CD8, CD4, CD79a, CD20 or CD57. Inset: higher magnification view of the boxed areas. A positive cellular staining was obtained for each of these leukocyte markers attesting the validity of the methodology used for the detection of lymphocyte subsets in our *postmortem* human brain material. Note that omission of the primary antibody resulted in absence of staining (Omit). Scale bar: 100 µm (insets: 30 µm).

Supplemental Figure 2

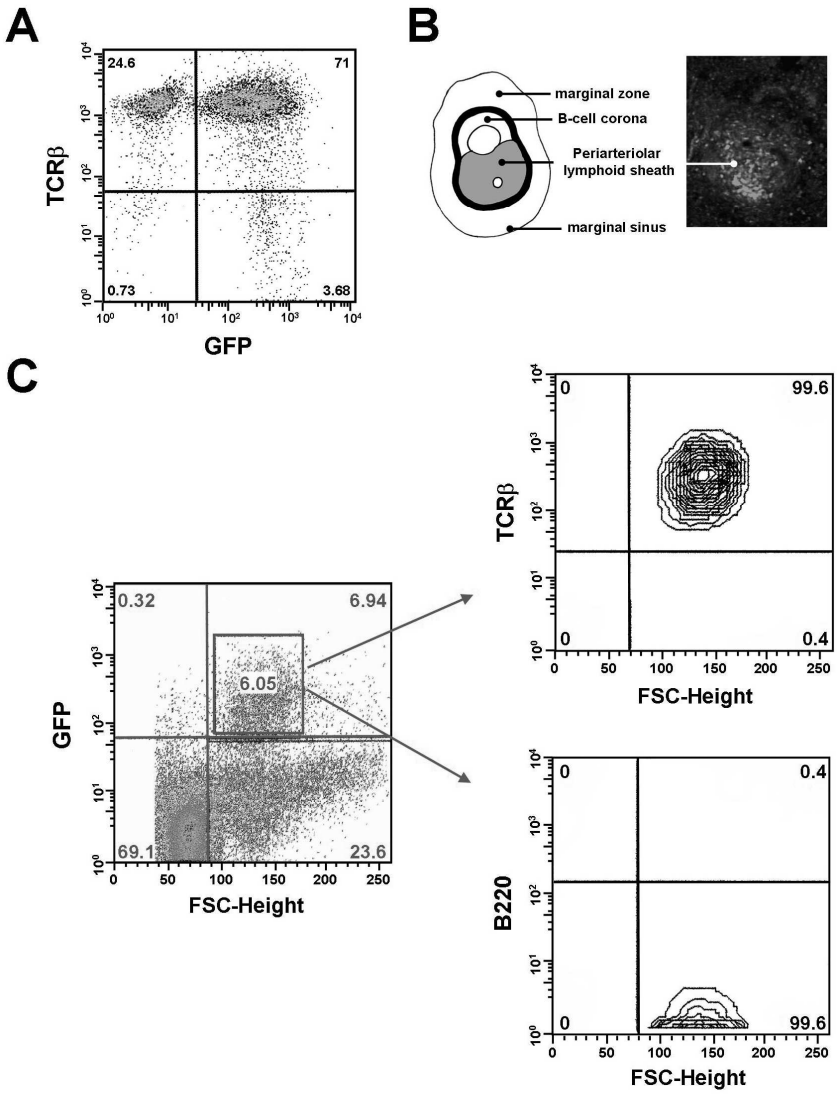

Supplemental Figure 2: Characterization of GFP+ T-cell-reconstituted *Rag1-/-* mice (**a**) Flow cytometry analysis of TCRb and GFP expression in positively selected cells from Tie2-Cre+/ZEG+ mouse lymph nodes shows more than 95% enrichment in T-cells. (**b**) Schematic view of white pulp in a transverse section of mouse spleen (left). Note that the periarteriolar lymphoid sheath (PALS) is made up of T cells. (Right) GFP+ cells in a transverse section of spleen from a GFP+ T-cell-reconstituted *Rag1-/-* mouse at 4 weeks post-transfer. Most of the GFP+ cells are located within the PALS. (**c**) Representative frequency of T- (TCRb+) and B-cells (B220+) among gated GFP+ cell subsets in lymph nodes from a MPTP-treated GFP+ T-cell-reconstituted *Rag1-/-* mouse. GFP+ cells are almost exclusively of T-cell subtype without major B-cell contamination.

Supplemental Figure 3

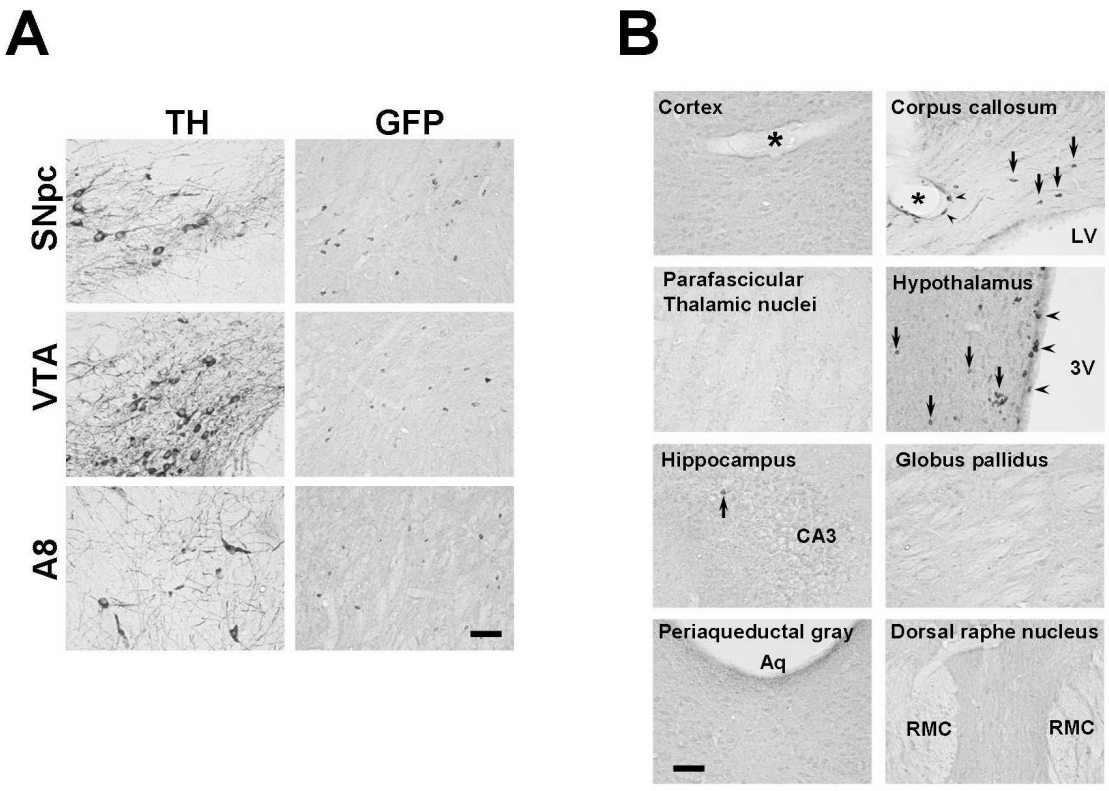

Supplemental Figure 3: Site specific recruitment of GFP+ T-cells in the brain of MPTP-intoxicated mice. (**a**) GFP+ T-cell infiltration (sections immunostained for GFP, right panels) in DN-containing brain areas (sections immunostained for TH, left panels) including the SNpc, the catecholaminergic cell group A8 and the ventral tegmental area (VTA). Scale bar: 80 µm. (**b**) MPTP-induced T-cell extravasation in various brain areas. Except in the corpus callosum and hypothalamus, infiltrated GFP+ T-cells (arrows) are rarely found in other brain structures. Asterisk: blood vessels, LV, lateral ventricle, 3V, third ventricle, Aq, Sylvius aqueduct, RMC, magnocellular part of the red nucleus. Scale bar: 80 µm.

Supplemental Figure 4

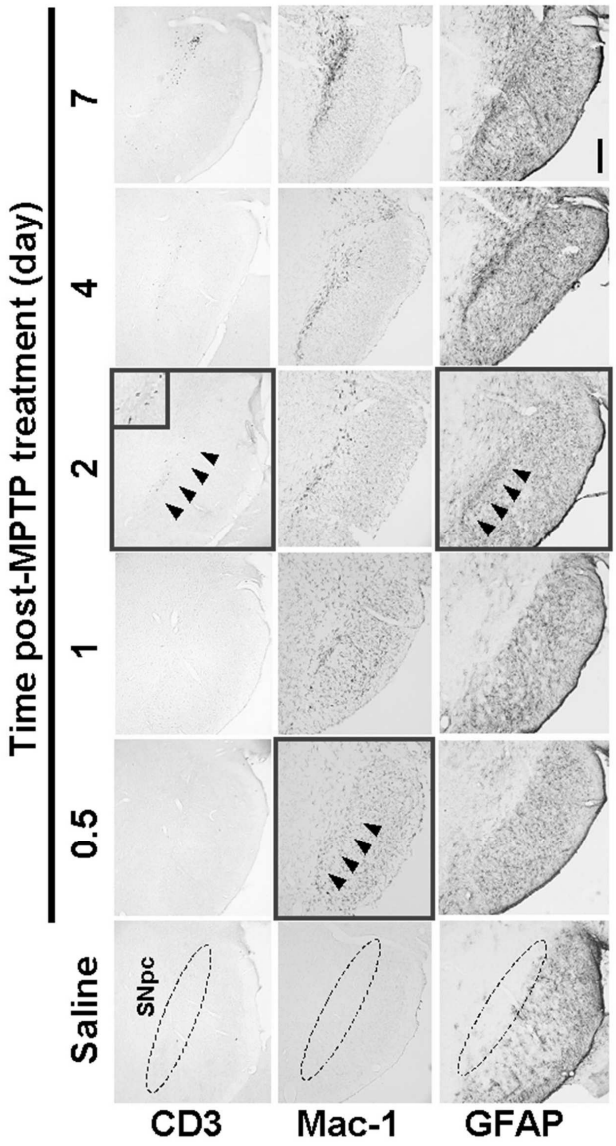

Supplemental Figure 4: Kinetics of T-cell brain infiltration and glial cell activation in the SNpc of MPTP-intoxicated mice. Representative photomicrographs of mesencephalic sections immunostained for CD3 (upper panels), Mac-1/CD11b (middle panels) and GFAP (lower panels) from saline- or MPTP-treated mice sacrificed at 12hr, 1, 2, 4 and 7 days after toxin exposure. The SNpc is delineated by dashed line. Red-circled photomicrographs indicate the earliest time point at which CD3+ T-cells, Mac-1+ activated microglial cells or GFAP+ astrocytes can be substantially detected in the SNpc (arrowheads). Inset in day 2 CD3 picture shows CD3+ T-cells at higher magnification. Note that microglial cell activation following MPTP-induced nigrostriatal pathway injury precedes T-cell infiltration and astrogliosis. Scale bar: 300 µm.

Supplemental Figure 5

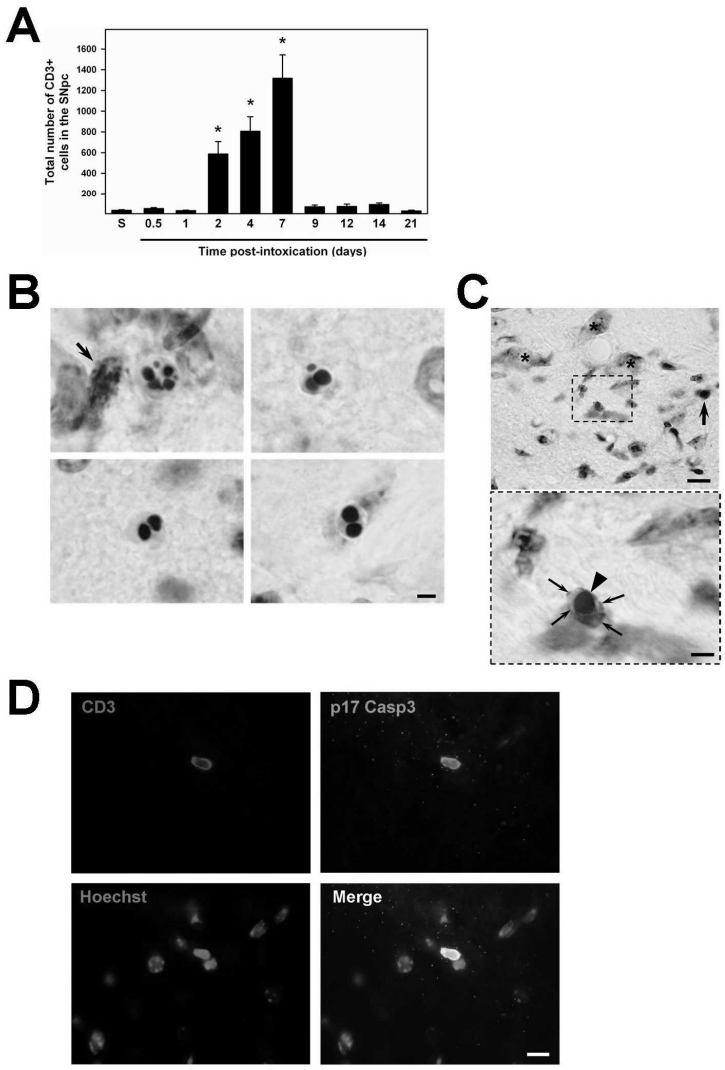

Supplemental Figure 5: Evidences for CD3+ T-cell apoptosis in the SNpc following MPTP intoxication. (**a**) Quantification of the total number of CD3+ T-cells in the SNpc at different time points after MPTP exposure. S: saline-treated controls. Each data point represents the mean ± SEM of 5-13 brains per group. *, $P < 0.01$, compared with saline-treated controls (Tukey *post hoc* analysis). (**b**) CD3 immunostaining with thionin counterstaining on mesencephalic sections from MPTP-treated mice sacrificed at day 7 and day 9 after intoxication. Photomicrographs at the level of the SNpc showing cases of pyknotic cells with well-defined thionin-stained chromatin clumps. A CD3+ T cell (arrow) with well preserved thionin-stained nucleus is shown in the vicinity of an apoptotic cell. Scale bar: 4 µm (**c**) Same experimental conditions as in (b). Illustration of a CD3+ apoptotic cell within the SNpc at day 7 after MPTP. Arrow: normal CD3+ T cell, Asterisks: neurons. Magnification of the dashed box area shows a T cell with CD3 staining (arrows) and a condensed thionin-stained nucleus typical of apoptosis. Scale bar: 10 µm, dashed box: 4 µm. (**d**). Double immunofluorescent staining for CD3 (red) and p17 caspase-3 (green) with Hoechst counterstaining (blue). Scale bar: 8 µm.

Supplemental Figure 6

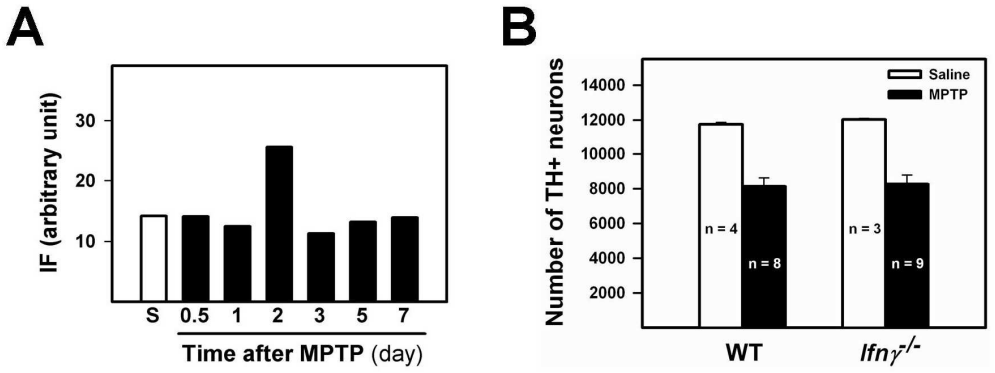

Supplemental Figure 6: Expression and role of IFN-γ in MPTP-induced nigrostriatal pathway injury. (**a**) Time course of IFN-γ expression in the ventral midbrain following MPTP intoxication as determined using antibody array glass chip (see Methods for details). IF: intensity of fluorescence, S: saline-treated mice. Note the up-regulated expression of IFN-γ two days after MPTP exposure. (**b**) Quantification of total TH+ DN neurons in the SNpc at day 7 after MPTP (4x18mg/kg) or saline treatment in WT and *Ifnγ-/-* mice. Data represent the mean number of total nigral TH+ DNs ± SEM for the indicated number of animals. Mice deficient in IFN-γ and their WT littermates are equally sensitive to MPTP-induced dopaminergic cell death ($P = 0.85$, Student's *t* test).